UC Berkeley
UC Berkeley Previously Published Works

Title

A DFT Investigation of the Mechanism of Propene Ammoxidation over α-Bismuth Molybdate

Permalink

Journal

ISSN

Authors

Licht, Rachel B
Bell, Alexis T

Publication Date

DOI

Peer reviewed

A DFT Investigation of the Mechanism of Propene Ammoxidation over α-

Bismuth Molybdate

Rachel B. Licht and Alexis T. Bell*

Department of Chemical and Biomolecular Engineering
University of California
Berkeley, CA 94720-1462
and
Chemical Sciences Division
Lawrence Berkeley National Laboratory
Berkeley, CA 94720

*To whom correspondence should be addressed: alexbell@berkeley.edu

Abstract

The mechanisms and energetics for the propene oxidation and ammoxidation occurring on the (010) surface of $Bi_2Mo_3O_{12}$ were investigated using density functional theory (DFT). An energetically feasible sequence of elementary steps for propene oxidation to acrolein, propene ammoxidation to acrylonitrile, and acrolein ammoxidation to acrylonitrile are proposed. Consistent with experimental findings, the rate limiting step for both propene oxidation and ammoxidation is the initial hydrogen abstraction from the methyl group of propene, which is calculated to have an apparent activation energy of 27.3 kcal/mol. The allyl species produced in this reaction is stabilized as an allyl alkoxide, which can then undergo hydrogen abstraction to form acrolein or react with ammonia adsorbed on under-coordinated surface Bi^{3+} cations to form allylamine. Dehydrogenation of allylamine is shown to produce acrylonitrile, whereas reaction with additional adsorbed ammonia leads to the formation of acetonitrile and hydrogen cyanide. The dehydrogenation of allyalkoxide species is found to have a significantly higher activation barrier than reaction with adsorbed ammonia, consistent with the observation that very little acrolein is produced when ammonia is present. Rapid reoxidation of the catalyst surface to release water is found to be the driving force for all reactions involving the cleavage of C-H or N-H bonds, since practically all of these steps are endothermic.

1. Introduction

Approximately 25% of the organic chemical building blocks produced commercially are obtained via heterogeneously catalyzed partial oxidation of alkanes or alkenes.[1] Two of the most important examples of such reactions are propene oxidation to acrolein and propene ammoxidation to acrylonitrile:

$$C_3H_6 + O_2 \rightarrow C_3H_4O + H_2O$$

$$C_3H_6 + {}^3/_2\, O_2 + NH_3 \rightarrow C_3H_3N + 3\, H_2O$$
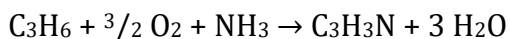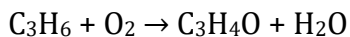
These reactions produce ~10 billion pounds/year each of acrolein, about 90% of which is directly converted to acrylic acid,[2] and of acrylonitrile,[3] which is used to produce plastics (e.g. ABS, SAN, NBR) and high volume commodity chemicals (e.g., acrylic fiber, acrylamide, adiponitrile). Both reactions occur with high intrinsic carbon selectivity over alpha bismuth molybdate $Bi_2Mo_3O_{12}$, ~70% for propene oxidation to acrolein and ~60% for propene ammoxidation to acrylonitrile.[4] While industrial catalysts have been engineered over the past 60 years to attain even higher product yields, the majority of the catalysts used still contain bismuth and molybdenum as key elements.[1]

The mechanism and kinetics of propene oxidation and ammoxidation have many features in common. The apparent activation energy for both reaction is virtually the same (~22 kcal/mol) and the rate of both reactions is first order in propene partial pressure, zero order in oxygen partial pressure, provided the feed concentration of oxygen is stoichiometric or greater, and zero order in ammonia partial pressure (for propene ammoxidation).[4,5,6,7,8] Both deuterium [9,10,11] and carbon-13 [12,13,14] labeling experiments provide compelling evidence that the rate-determining step for both reactions is the same, and involves hydrogen abstraction from the methyl group of propene to produce loosely adsorbed allyl

species. Since the initial propene activation step is rate-determining, it is difficult to probe the subsequent reactions and, therefore, multiple theories have been presented to account for the formation of acrolein and acrylonitrile. In particular, while acrolein is produced in only low concentrations when ammonia is present and is not thought to be an intermediate on the primary path to acrylonitrile,[4,5,8] it is not clear at what point the common intermediate diverges to become either acrolein or acrylonitrile.

Insights into the activation of propene on $Bi_2Mo_3O_{12}$ have also been obtained from density functional theory calculations. Despite many of the inherent challenges of modeling reducible transition metal oxides with DFT because of problems with electron self-interaction error, we have found that reasonably accurate estimates of oxide semi-conductor band gaps, lattice parameters, heats of molecular adsorption and reaction energies can be obtained at a reasonable cost using the M06-L functional[15] implemented for a periodic boundary system representation of the (010) surface of $Bi_2Mo_3O_{12}$.[16] Using this approach, we have investigated the surface chemistry involved in the oxidation of propene to acrolein. This work has shown that the most active site for the rate-limiting propene activation step is a surface molybdenyl oxo that is mildly perturbed electronically by a nearby bismuth cation,[16, 17] and not an oxygen atom bound to bismuth as had been proposed previously. [18, 19, 20] The apparent activation energy calculated for the abstraction of a hydrogen atom from the methyl group of propene by this oxo group is 27.9 kcal/mol.[16] This value is in reasonably good agreement with the experimentally measured value of ~22kcal/mol, considering the technical difficulties of associated with the calculations noted above. The theoretical finding that the active site is an oxygen atom bound only to molybdenum is consistent with our experimental *in situ* XANES results, which show that,

even under extremely reducing conditions (exposure to pure propene for 24 h at 713 K), only molybdenum is reduced from 6+ to 4+ and bismuth remains in the 3+ oxidation state.[7]

Experiments with $^{18}O_2$ have demonstrated that the acrolein O originates from the catalyst, and not from gas phase oxygen,[21,22] leading to a general consensus that, after the initial hydrogen abstraction, the nascent allyl radical first inserts into a molybdenyl oxo $Mo^{6+}=O$ to form an allyl alkoxide species, which then undergoes a hydrogen abstraction followed by desorption of acrolein leaving a reduced Mo^{4+} site.[17,20] Based on calculations conducted using a Mo_3O_9 cluster, Goddard *et al.* have estimated that both the hydrogen abstraction step and the release of acrolein to leave a Mo^{4+} cation are demanding steps with activation barriers of 35.6 kcal/mol and 31.9 kcal/mol, respectively. The authors proposed that acrolein release may be facilitated by concurrent adsorption of gas phase oxygen on molybdenum, thereby maintaining molybdenum in a higher oxidation state and resulting in acrolein release being energetically favorable. [23]

Grasselli *et al.* have proposed, by analogy with the mechanism for propene oxidation, that propene ammoxidation involves the insertion of an allyl radical into a molybdenyl imido $Mo^{6+}=NH$ group, followed by three hydrogen abstraction steps.[20] The authors proposed that the catalyst surface is dominated by imido groups, formed by the reaction of NH_3 with Mo=O groups, since little acrolein is produced during propene ammoxidation.[24] Using this scheme as a basis, Goddard *et al.* have explored the reaction of allyl radicals with a Mo_3O_9 cluster in which 1, 2, 3 or 6 of the oxo groups is replaced with imido groups. This work showed that hydrogen abstraction by an imido group is ~8 kcal/mol more favorable than by an oxo group, and that a spectator imido bound to the same Mo^{6+} further facilitates hydrogen abstraction by an additional ~15 kcal/mol. [25] It is notable, however, that the production of an imido

group and water by reaction of ammonia with an Mo oxo group is endothermic by 13.7 kcal/mol, indicating that the imido groups will be unstable to hydrolysis. [26]

Given the unfavorable thermodynamics for imido group formation on the surface of bismuth molybdate, these groups are not likely to be present in high concentration during propene ammoxidation, since this reaction produces a considerable amount of water. Consistent with this reasoning, we have recently reported that co-feeding water together with propene, oxygen, and ammonia has a negligible effect on the rate of acrylonitrile formation, leading to the conclusion that imido groups are unlikely to be responsible for C-N bond formation.[4] We have proposed, instead, that the formation of C-N bonds occurs via the reaction of allyl alkoxide groups (produced by addition of an allyl radical to a Mo=O group) with ammonia adsorbed on Bi^{3+} cations via sigma donation of electron density from the lone pair on the nitrogen atom of NH_3. The product of this step was proposed to be adsorbed allylamine. While this compound was not observed as a stable product, introduction of allylamine with ammonia and oxygen under conditions used to carry out propene ammoxidation resulted in a product distribution very similar to that observed during propene ammoxidation.[4]

A small amount of acrolein has been observed during propene ammoxidation under conditions of differential conversion; however, the majority of the acrolein produced undergoes facile secondary reaction to acrylonitrile with an activation energy of ~7 kcal/mol.[4,5,8] Finally, acetonitrile and hydrogen cyanide (HCN) are important byproducts of propene ammoxidation. Our experimental studies have shown that these products are produced from propene in an approximately constant ratio of 5 HCN: 2 acetonitrile, and together account for ~30% of the reacted propene.[4]

The aim of the present investigation was to carry out a detailed analysis of the reaction pathways involved in the oxidation and ammoxidation of propene. Specific objectives were to identify the elementary steps for the formation of both acrolein and acrylonitrile during propene ammoxidation, the pathway by which acrolein is subsequently converted to acrylonitrile, and the pathways by which the byproducts acetonitrile and hydrogen cyanide are formed. The objectives were pursued by analysis of the energetics for the reaction pathway proposed on the basis of our experimental studies.[4] Periodic-boundary, density functional theory (DFT) calculations were conducted on the (010) surface of $Bi_8Mo_{12}O_{48}$. Given the very large number of structures investigated, we only considered the reaction barriers for three key steps: (1) hydrogen abstraction from propene, the rate-limiting step that is common to propene oxidation and ammoxidation; (2) hydrogen abstraction from surface allyl alkoxide species to produce adsorbed acrolein; and (3) the reaction of allyl alkoxide species with adsorbed ammonia to produce allylamine. All other aspects of the reaction pathways were explored by examining the energies of reaction.

2. Theoretical Methods

All calculations were performed using the Vienna *Ab initio* Simulation Package (VASP)[27] version 5.3.5 using the PBE[28] and M06-L[15] functionals. Plane wave basis sets[29] were used to model valence electrons and projector augmented wave (PAW) functions[30,31] were used to model the core electrons. The PAW cores were designed for a plane wave cutoff energy of 400 eV and this cutoff was used for all calculations. We used 240 bands in order to capture the 200 electron pairs present in $Bi_8Mo_{12}O_{48}$, the lowest energy unoccupied bands involved in reactions, and the additional electrons introduced with the reactants.

Convergence tests with respect to k-point mesh revealed that 3x2x2 k-points are sufficient to simulate the bulk $Bi_8Mo_{12}O_{48}$ with the M06-L functional.[16] Energies were converged with a Gaussian energy smearing of 0.05 eV.

The bulk atomic positions of $Bi_8Mo_{12}O_{48}$, which is one unit cell of alpha bismuth molybdate, were taken from literature[32] and allowed to relax at a series of fixed volumes[16]. The Burch-Murnaghan Equation of State[33] was used to fit the data of energy versus volume to calculate the cell volume with the minimum energy. The atoms were then allowed to relax at this fixed minimum energy volume until the total energy converged to within 0.1 meV. The optimized cell volume from this method is ~2.3% larger than the experimental unit cell volume.[16] In order to generate the lowest energy (010) surface, 14 Å of vacuum was introduced above the bulk $Bi_8Mo_{12}O_{48}$ atoms and the top two layers of the four layer unit cell were allowed to relax to a convergence of 0.5 meV with 3x1x2 k-points, while the bottom two-layers were fixed in their bulk positions to simulate the bulk oxide below the surface. The Minnesota family of functionals requires a fine integration grid to provide accurate energies,[34] therefore an integration grid of 90 x 288 x 144 was used in all calculations.

To model reactant and product structures, the positions of both the reactants and the relevant atoms at the active site were optimized initially with the less-computationally-intensive PBE functional and with 1x1x1 k-points. Once a structure was optimized to within 0.5 meV, the entire surface was allowed to relax using the M06-L functional with 3x1x2 k-points until the final structure converged to within 1 meV. The charge density and wave function from a single point PBE calculation was always used as an initial guess for M06-L calculations, since the M06-L functional performs poorly with the default random number initial guess of the wave function.

The Nudged Elastic Band (NEB) method[35] was used to calculate the three reaction barriers we investigated. As mentioned in the Introduction, the transition state for the rate-limiting hydrogen abstraction from propene has been found to be the singlet-triplet spin crossing.[17] Therefore, for this barrier, we first optimized a spin-relaxed pathway until the forces on all the atoms were less than 0.1 eV/Å. We then ran two single-point NEBs on the final optimized pathway geometries, one confined in the singlet state and one confined in the triplet state, and extracted the forces and energies. From these data, we generated cubic splines representing the singlet and triplet potential energy surfaces and found the spin crossing point. We interpolated along the pathway to find the geometry at the spin crossing point, and verified that the resulting geometry had the same energy in the singlet and triplet spin states. The probability of spin-crossing due to spin-orbit coupling is known to be almost 100% for this system,[17] therefore the highest energy along the true spin-coupled pathway was found by subtracting the spin-orbit coupling energy (4.6 kcal/mol) estimated from values reported in the literature[36] from the crossing point of the two fixed spin pathways. Additional details on this method can be found in our previous study of this subject.[17] For the reaction barriers of allyl alkoxide to acrolein and allyl alkoxide plus ammonia to allylamine, the initial and final states had the same spin state (doublet), so spin-crossing calculations were not necessary. For both of these pathways, the Climbing Image NEB method, optimized until the forces on each atom were less than 0.5eV/Å, was used to find the transition state.[37]

We also performed a few bond dissociation energy (BDE) and gas phase free energy calculations using the Q-Chem simulation package, version 4.3.2.[38] Both types of calculations

were performed using the ωB97X-D functional and the 6-311++G(3df,3pd) basis set for final energy values.

3. Results and Discussion

3.1 Catalyst Active Site

Fig. 1 depicts a section of top layer of the (010) surface of $Bi_2Mo_3O_{12}$ from our optimized slab model, with relevant distances indicated. The highlighted sites **A** and **B** are both oxygen atoms formally doubly bonded to molybdenum cations and electronically perturbed by neighboring bismuth atoms. Since we have found previously that unperturbed molybdenyl oxo groups are less active than Bi-perturbed ones, and that bismuth-molybdenum bridging oxygen sites are even less active than either of the molybdenum oxos,[17] we did not consider reaction at any other sites. However, since site **A** is slightly closer to the nearby bismuth than site **B** (2.8 Å and 3.0 Å respectively) and thus has a stronger electronic perturbation, site **A** is the most active surface site and was used as the primary site for our calculations.

As indicated in Fig. 1a, sites **A** and **B** repeat in the order **A-B-A-B** etc. in a line on the (010) surface. As the oxo groups distort to the side to reduce the repulsive interaction with the bismuth lone pair, they become closer together on one side and further apart on the other side (3.3 Å and 5.1 Å respectively) on the surface optimized at 0 K. At reaction temperatures, the exact location of each oxo group will fluctuate, but each one will always have two neighboring oxos 3-5 Å away. We invoke the utilization of two sites for many of the reactions below, since this 3-5 Å gap is small enough that the hydrocarbon can easily span it. One unit cell of $Bi_2Mo_3O_{12}$ contains one **A** and one **B** surface site, plus one bridging molybdenum site,

such that there are 3 molybdenum atoms and 2 bismuth atoms at the surface. To depict our proposed mechanisms, we use a top-down view representation of the unit cell surface with the primary **A** site indicated in black and the secondary neighboring **B** site in grey (see Fig. 1b). Since the unit cell model is periodic, the secondary **B** site used for calculations that require two sites is actually both on the close (3.3 Å) side and on the far (5.1 Å) side of the primary **A** site.
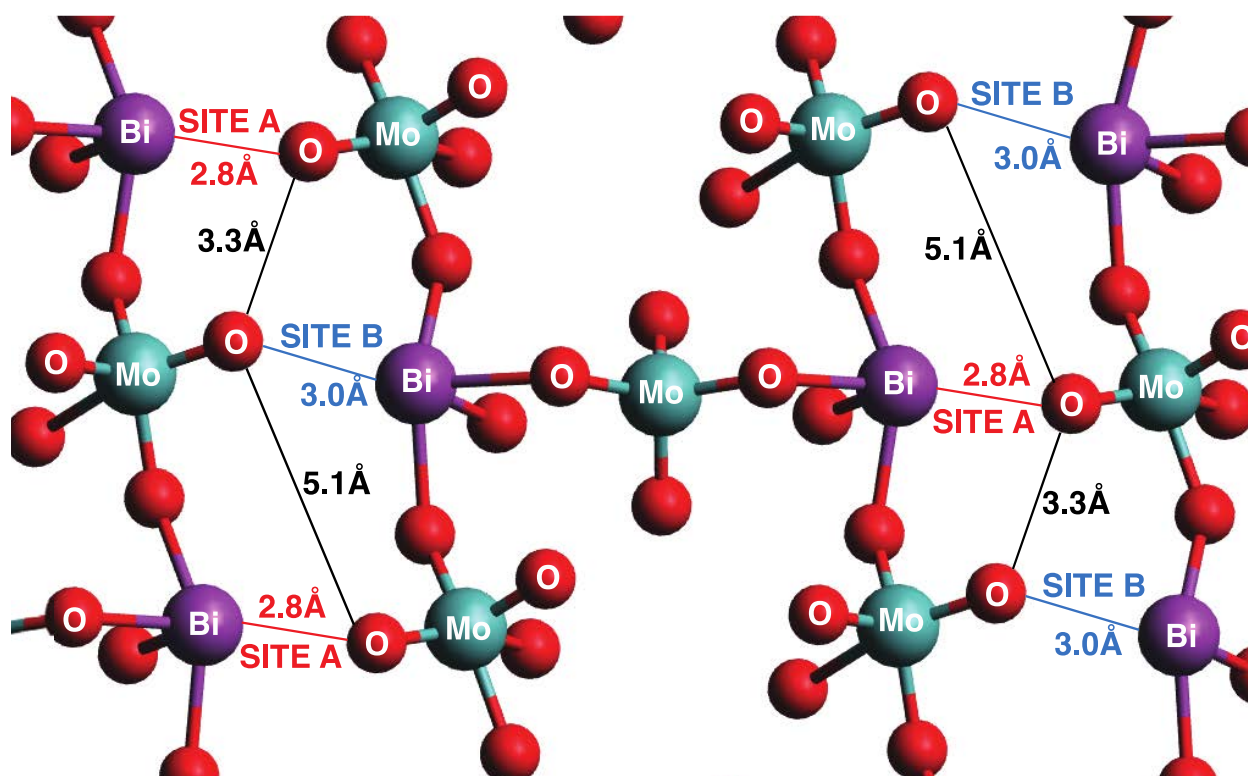

Fig. 1 (a) Top-down view of the top layer of optimized (010) surface of $Bi_2Mo_3O_{12}$, with relevant distances indicated in Å and the key **A** and **B** sites labeled. All red balls represent oxygen atoms, but only those marked with an "O" are at the surface. (b) Simplified representation of the same surface used in the remainder of this paper.

3.2 Catalyst Reoxidation

During propene (amm)oxidation, hydrogen atoms are removed from propene and from ammonia by the catalyst, resulting in reduction of the catalyst surface. In order to complete the catalytic cycle, pairs of hydrogen atoms must combine with oxygen atoms

generated by dissociation of molecular oxygen in order to release water. Previous authors have assumed that all hydrocarbon conversion steps occur before the catalyst surface in reoxidized in the final step of the catalytic cycle. However, this way of viewing the reaction mechanism is not physically correct, since, as noted below, experiments show that the catalyst is reoxidized at rate that is much faster than the rate of reduction. We note further that assuming that reoxidation occurs at the end of all steps leading to products is unrealistic for calculations of propene ammoxidation to acrylonitrile over a $Bi_8Mo_{12}O_{48}$ unit cell, which only has four surface molybdenyl oxo units (only two of which are the most active bismuth-perturbed oxos) on which to put H atoms. During propene ammoxidation, six H atoms are removed from propene and ammonia (3 from each reactant), and consequently there are simply not enough low energy locations to store all of the liberated H atoms.

XANES experiments reported by our group indicate that even under extreme reducing conditions (exposure to 1atm pure propene for 24 h at 713 K) only molybdenum is reduced and only to Mo^{4+}, and that under standard propene oxidation conditions (O_2/C_3H_6 = 1 and T = 713 K) both metals remain in their highest oxidation state.[7] Previous studies have shown that the rate of propene consumption during both oxidation and ammoxidation is independent of the oxygen partial pressure, as long as it is supplied at stoichiometric or higher concentrations. These observations indicate that the rate of catalyst reoxidation by oxygen is faster than the rate of catalyst reduction by propene.[4,8,39] Moreover, experiments conducted in the absence of oxygen demonstrate that, for a short period of time, the rate of propene oxidation is the same whether or not oxygen is provided, indicating that highly mobile O^{2-} ions coming from the bulk of the catalyst can participate in reactions.[40,41,42] The participation of lattice oxygen atoms is further supported by experiments in which a mixture

of $^{16}O_2$ and $^{18}O_2$ is fed over bismuth molybdate and no evidence is found for $^{16}O^{18}O$ formation, indicating that dissociation of gas-phase oxygen is favorable and irreversible. [43] Taken together, these observations lead to the conclusion that, under standard reaction conditions with a feed containing at least a stoichiometric concentration of oxygen, the catalyst surface is very close to being completely oxidized and that surface oxygen atoms are highly mobile and can react with hydrogen atoms produced by the cleavage of C-H or N-H bonds to generate water.

Therefore, in all our calculations, as soon as a hydrogen atom is liberated from propene or ammonia, it is removed in a reoxidation step involving ¼ O_2 to produce ½ H_2O. Leaving the H atom on the surface until another H is liberated not only blocks the only adjacent H abstraction site competent to do chemistry, but results in an unphysical situation in which $^1/_3$ of the surface of molybdenum cations are reduced. Continuing to perform reactions on partially reduced surfaces becomes more and more unfavorable. In order to assure that all calculations relate to a fully oxidized surface, as indicated by experimental results, we immediately remove released H atoms to mimic the experimentally-observed rapid reoxidation of the catalyst.

3.3 Relevant Hydrogen Bond Dissociation Energies

Table 1 shows the DFT-calculated C-H, N-H and O-H bond dissociation energies (BDEs) for a number of gas phase species relevant to the chemistry of propene oxidation and ammoxidation. The BDE is difference between the sum of the energy of a hydrogen radical and the optimized remaining radical fragment and the energy of the optimized parent molecule. As will be discussed in more detail below, the entries shown in black represent C-H bonds that are weak enough to be broken by $Bi_2Mo_3O_{12}$ in the course of propene oxidation

and ammoxidation. By contrast, the entries shown in red represent C-H and N-H bonds are too strong to be broken by the catalyst. The BDE cutoff for $Bi_2Mo_3O_{12}$ is ~94 kcal/mol, since the C_1-H bond of propene is broken in the rate-limiting step (BDE 92.7 kcal/mol) and acrolein is a stable product (weakest BDE 95.3 kcal/mol). The fact that the intrinsic hydrogen abstraction ability of $Bi_2Mo_3O_{12}$ falls between the two values suggests why $Bi_2Mo_3O_{12}$ is a good catalyst for propene oxidation, since a more active catalyst could break the C_1-H bond of acrolein to react it all the way to CO_x and would thus be a non selective, while a less active catalyst would not be able to activate propene to begin the reaction. The relevance of bond dissociation energies is also supported by our prior work on the reactivity of different hydrocarbons (propane, propene, 1-butene, 2-butene and isobutene) over $Bi_2Mo_3O_{12}$, which showed a correlation between the strength of the weakest C-H bond and the apparent activation energy of that compound in either oxidative dehydrogenation or partial oxidation.[44]

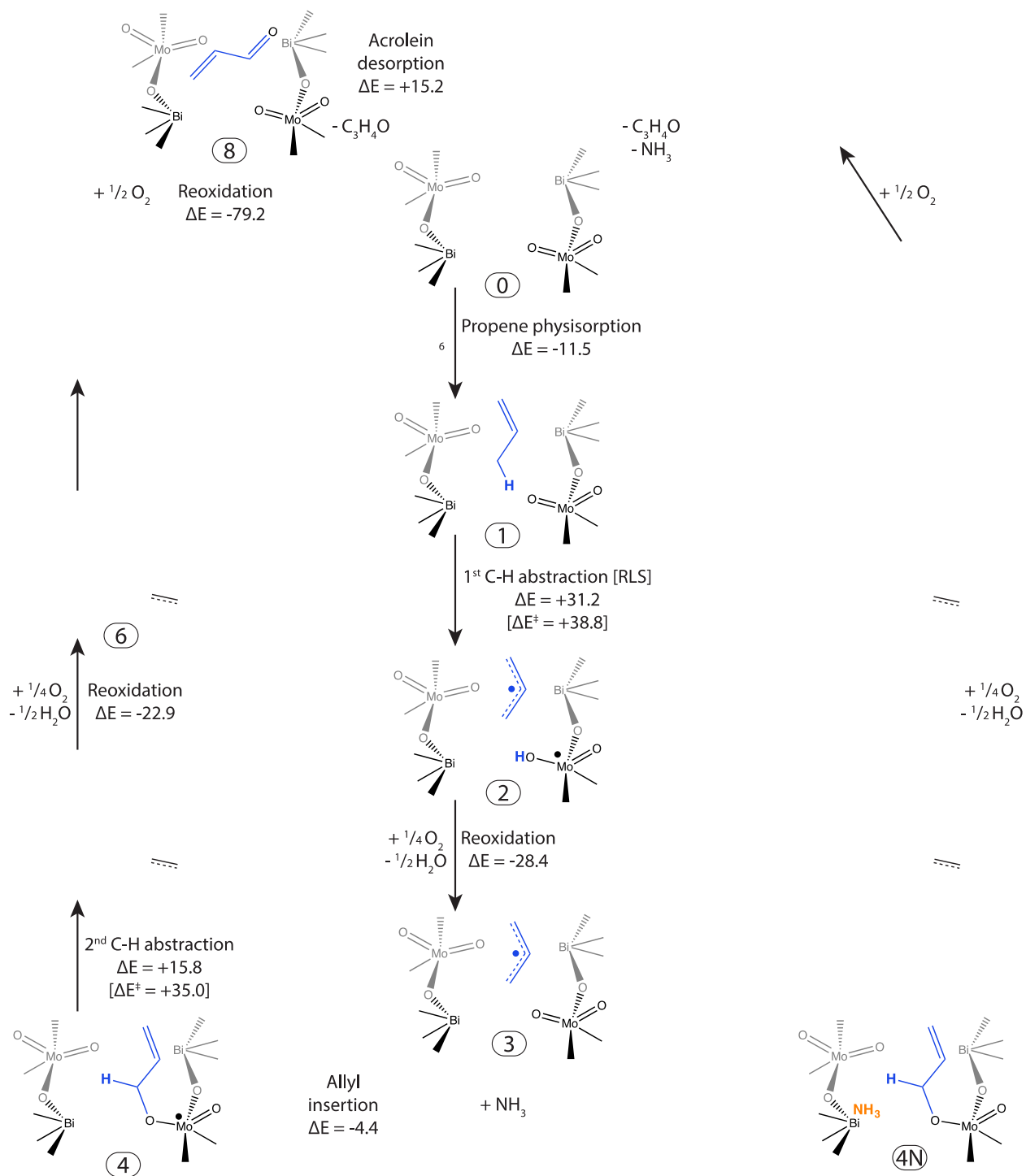Table 1. Gas phase bond dissociation energies

	BDE [kcal/mol]			
Molecule	**C_1–H**	**C_2–H**	**C_3–H**	**N–H or O-H**
C_3H_2=C_2H-C_1H_3 Propene	92.7	114.2	119.3	--
C_3H_2=C_2H-C_1H_2-OH Allyl alcohol	85.1	115.0	117.4	(O-H) 111.1
C_3H_2=C_2H-C_1H=O Acrolein	95.3	118.4	118.0	--
C_3H_2=C_2H-C_1H_2-NH_2 Allylamine	82.3	114.9	117.8	(N-H) 106.4

$C_3H_2=C_2H-C_1H=NH$ 2-propen-1-imine	102.1	109.9	117.7	(N-H) 96.7
$C_3H_2=C_2H-C_1\equiv N$ Acrylonitrile	--	111.2	119.5	--
$C_2H_3-C_1\equiv N$ Acetonitrile	--	101.9	--	--
$HC_1\equiv N$ Hydrogen Cyanide	135.2	--	--	--
$C_3H_2=C_2H-C_1H(-OH)(-NH_2)$ 2-propen-1-ol-1-amine	80.6	116.2	117.3	(N-H) 109.0 (O-H) 111.8
$C_3H_2=C_2H-C_1H(-OH)(=NH)$ 2-propen-1-ol-1-imine	--	116.5	117.3	(N-H) 109.6 (O-H) XX
$C_3H_2=C_2H-C_1(=O)(-NH_2)$ Acrylamide	--	114.2	117.1	(N-H) 117.5
NH_3 Ammonia	--	--	--	(N-H) 114.1

3.4 Propene Oxidation to Acrolein

The proposed elementary steps and corresponding energy profile for propene oxidation to acrolein are shown in Scheme 1 and Fig. 2, respectively. In agreement with experiment, the initial activation of propene to produce a physisorbed allyl radical (steps **0** → **3**) is rate-limiting and is common to both propene oxidation and ammoxidation. The subsequent steps (**3** → **8**) are very similar to those that have been proposed by previous researchers.[7,17,20]

Acrolein desorption
ΔE = +15.2

-C_3H_4O

-C_3H_4O
-NH_3

8

+ $^1/_2 O_2$ **Reoxidation**
ΔE = -79.2

+ $^1/_2 O_2$

0

Propene physisorption
ΔE = -11.5

6

H

1

1st C-H abstraction [RLS]
ΔE = +31.2
[ΔE‡ = +38.8]

6

+ $^1/_4 O_2$ **Reoxidation**
- $^1/_2 H_2O$ ΔE = -22.9

HO

2

+ $^1/_4 O_2$
- $^1/_2 H_2O$

+ $^1/_4 O_2$ **Reoxidation**
- $^1/_2 H_2O$ ΔE = -28.4

2nd C-H abstraction
ΔE = +15.8
[ΔE‡ = +35.0]

3

H

Allyl insertion
ΔE = -4.4

+ NH_3

H

4

NH₃

4N

Scheme 1. Proposed elementary steps for propene oxidation to acrolein (ΔE in kcal/mol).
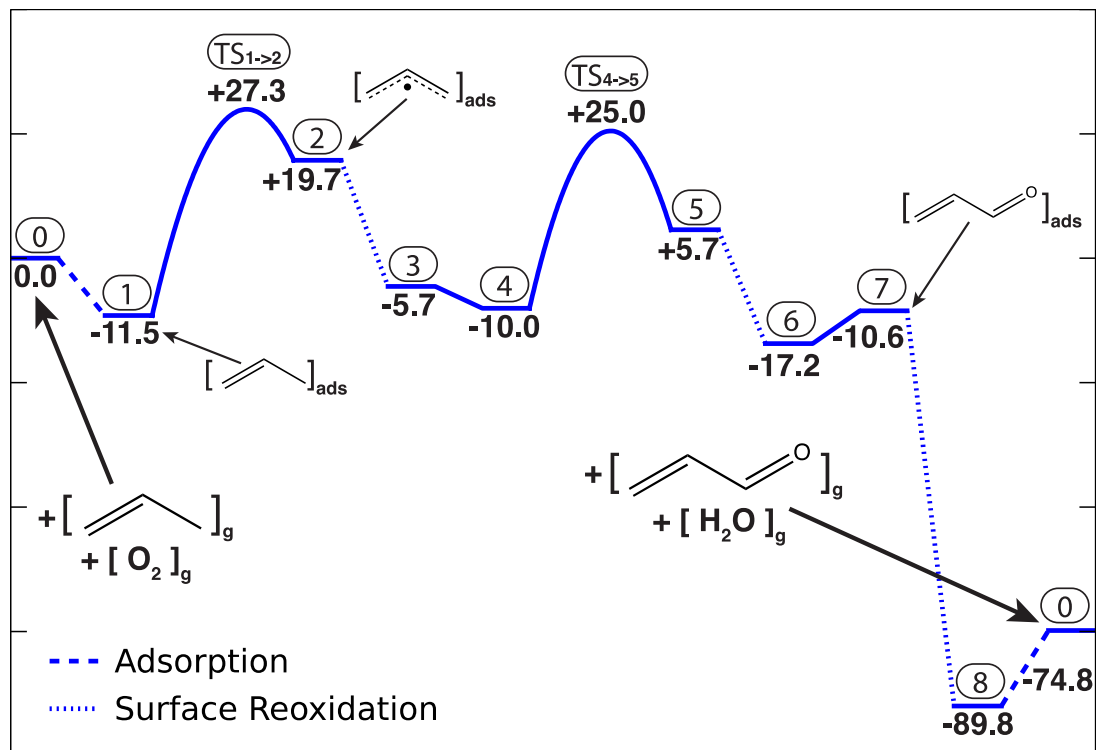
Fig. 2 Energy landscape for propene oxidation to acrolein. Encircled integers refer to structures in Scheme 1, bold numbers give the energy of each structure relative to the initial state.

The first step ($0 \rightarrow 1$) is propene physisorption. Previous DFT work in our group has reported an internal energy of adsorption over the (010) surface of $Bi_2Mo_3O_{12}$ to be -4.4 kcal/mol; however, that value is for a non-specific van der Waals adsorption above the space between sites **A** and **B**.[16] We have since found that the strongest propene adsorption site is directly over a surface Bi^{3+} atom at a distance of 3.33Å from the center of the double bond. In this adsorption mode, the pi-bonding electrons of propene donate electron density to the under-coordinated Bi^{3+} via a dative type interaction, resulting in a calculated internal energy of adsorption of -11.5 kcal/mol. For comparison, the experimental value for the enthalpy of adsorption of propene on bismuth molybdate is ~8 kcal/mol.[45]

The second step ($\mathbf{1} \rightarrow \mathbf{2}$) is abstraction of a hydrogen atom from the methyl group of propene by a bismuth-perturbed molybdenyl oxo. This key step has been previously investigated in our group and has been found to involve a singlet-triplet spin crossing transition state.[16,17] The reaction pathway starting from propene adsorbed over a neighboring Bi^{3+}, including the spin-singlet, spin-triplet and spin-coupled energy landscapes and geometries for the initial, spin crossing, and final state, is shown in Fig. 3. From its lowest energy adsorbed state, the propene moves parallel to the surface towards the molybdenyl oxo and passes over the hydrogen, then moves back to re-establish a dative interaction between the newly formed allyl radical and the bismuth cation. After subtracting the spin-orbit coupling energy from the spin-crossing point to attain the reaction pathway transition state, the value of ΔE_{TS} is found to be 38.9 kcal/mol. However, at reaction temperatures of ~673 K, the catalyst resting state is the bare catalyst surface; therefore, the propene adsorption energy is subtracted from the transition state energy to obtain an apparent activation energy of 27.3 kcal/mol. This value of the apparent activation barrier for the rate-limiting step is reasonably close to that measured experimentally for propene oxidation or ammoxidation (22 kcal/mol)[4].

The overall energy of reaction, ΔE_{rxn}, is very similar to the value of ΔE_{TS}, since the final state contains a high-energy radical species. In fact, we can see from the geometries on the right side of Fig. 3 that the transition-state geometry is very similar to the final-state geometry, with the molybdenum-oxygen bond highly elongated, the oxygen-hydrogen bond almost completely formed, the carbon-hydrogen bond already completely broken and the two carbon-carbon bonds of almost equal length. Consistent with the DFT-calculated final state $\mathbf{2}$, experimental studies have shown that acrolein produced from 1-^{13}C-propene

contains a 50/50 mixture of ^{13}C label in both terminal C positions of the product,[12] demonstrating that a free allyl species is produced is produced as an intermediate that can then react with equal probability at either end. While it appears that this reaction could easily go backward via **2 → 1**, this is unlikely to occur because of the rapid catalyst reoxidation that will remove the surface hydrogen in a very exothermic reaction to form water and the adsorbed allyl that can, in turn. As is clear from Fig. 2, the catalyst reoxidation to remove the hydrogen atom and leave an allyl radical over an oxidized surface (**2 → 3**) provides the thermodynamic driving force for propene activation.
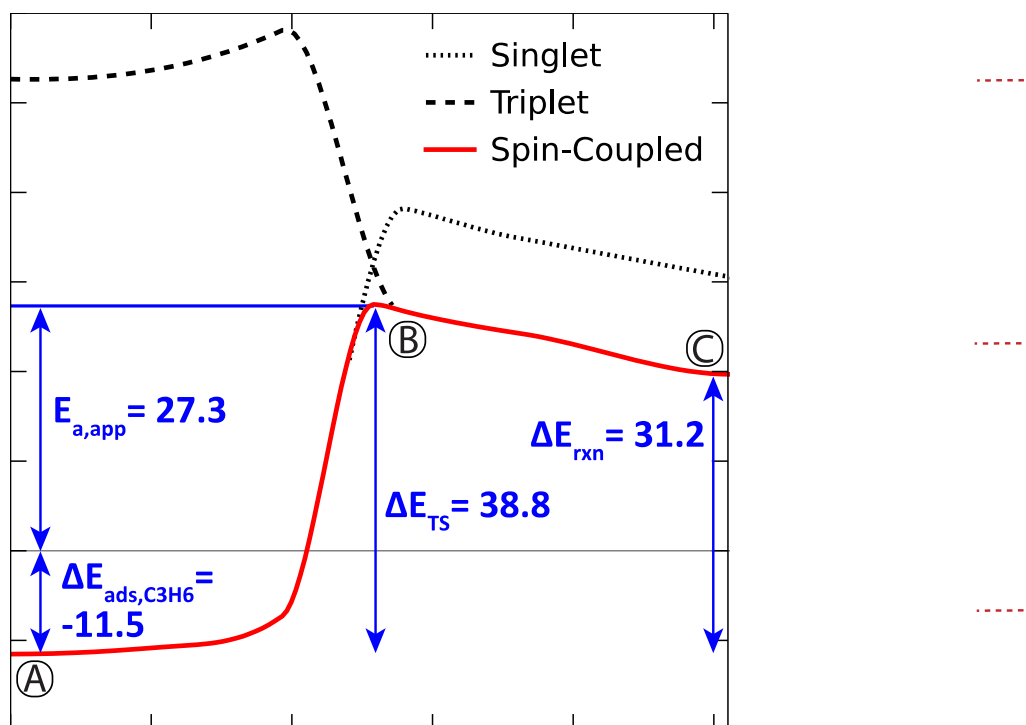
Fig. 3 Optimized spin-crossing reaction barrier for initial hydrogen abstraction from propene, with relevant energies annotated. Geometries for the initial state (A), spin-crossing transition state (B) and final state (C) are shown on the right, with relevant distances in Å indicated.

The next step (**3 → 4**) is insertion of allyl into a Mo=O bond to create an energetically favored surface allyl alkoxide species. Experimental studies conducted with $^{18}O_2$ in the gas phase have shown that the O in the product acrolein comes from the catalyst surface, and not from gas phase oxygen;[41] therefore, the C–O bond formed in step **3 → 4** remains in the final product. Considering the bond distances given in Table 2, we see that the allyl species (**3**) shares one unpaired electron among the three carbon atoms, resulting in two ~1.5 order bonds, while in **4**, there is a clear terminal C_2-C_3 double bond and single bonds between Mo and O, O and C_1, and C_1 and C_2.
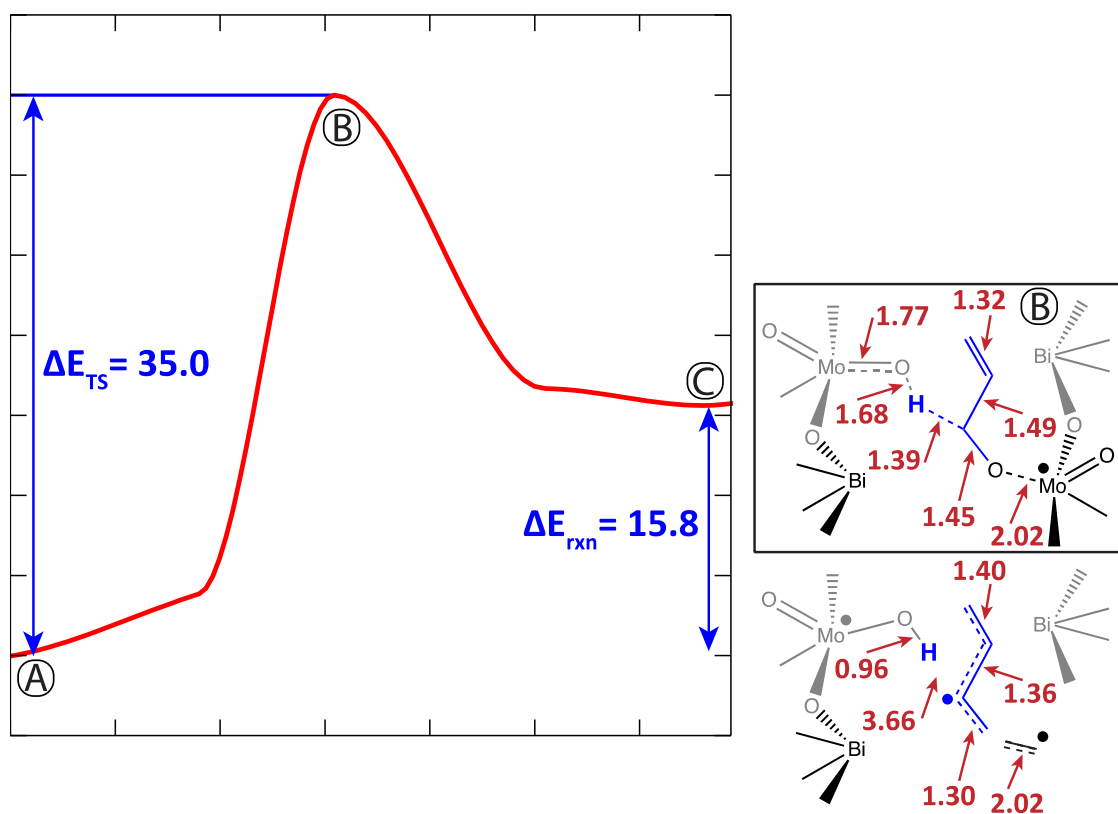
Fig. 4 Optimized reaction barrier for hydrogen abstraction from allyl alkoxide to produce coordinated acrolein, with relevant energies annotated. Geometries for the initial state (A), transition state (B) and final state (C) are shown on the right, with relevant distances in Å indicated.

20

The next step ($4 \rightarrow 5$) is the second most energetically demanding step after the initial, rate-limiting step of propene activation, and involves abstraction of an H atom from the allyl alkoxide species by a neighboring $O=Mo^{6+}=O$ group to produce Mo-coordinated acrolein and a reduced neighboring site. This hydrogen abstraction has previously been proposed by Grasselli[20] and by us[17] to occur via reaction with the other oxo group bound to the same molybdenum as the allyl alkoxide. However, our calculations show that the energy of this final structure ($C_3H_4O-Mo^{4+}-OH$) is 5 kcal/mol higher in energy than the final structure for hydrogen abstraction by a neighboring oxo group ($C_3H_4O-Mo^{5+}=O$ and $O=Mo^{6+}-OH$). Since the neighboring $O=Mo^{6+}=O$ group is close enough for the reaction to occur, we consider **5** to be the preferred end state. The reaction barrier energy and geometries are shown in Fig. 4.

As is clear from Fig. 4, abstraction of a hydrogen atom from allyl alkoxide to produce an adsorbed acrolein is quite difficult, and the value of ΔE_{TS} for this step is only slightly lower than that for the initial hydrogen abstraction from propene. While the BDE for allyl alcohol (see Table 1), which is an approximation of the allyl alkoxide species, is relatively low, the transition state is geometrically constrained since all species remain bound to the surface during reaction. From the bond distances shown in Fig. 4, we see that, during the reaction pathway, the allyl alkoxide fragment undergoes significant geometric distortion in order to move closer to the neighboring molybdenyl oxo group and vice versa. When hydrogen is transferred in the transition sate, the allyl alkoxide is still essentially intact with bond distances similar to those in the reactant state. However, the final state after hydrogen abstraction has all partial bond distances, demonstrating that there is electron delocalization across the entire acrolein fragment from molybdenum through the terminal carbon. There are formally three unpaired electrons in the final state as indicated in Fig. 4, however only

the one unpaired electron on the Mo that just abstracted the hydrogen radical from allyl alkoxide is isolated. The other two electrons can pair with the electrons in the carbon-carbon double bond or in the oxygen lone pairs to form the resonance structures $Mo^*–O–C_1^*–C_2=C_3$, $Mo^*–O–C_1=C_2–C_3^*$, $Mo^*–O^*=C_1–C_2=C_3$ or $Mo=O^*–C_1=C_2–C_3^*$, where * indicates an unpaired electron. Therefore, these two electrons on the acrolein species are actually paired and the lowest energy spin state of **5** is a doublet, not a quadruplet (only unpaired electron on the Mo with the newly formed hydroxyl). This is true for the reacting species over the entire reaction trajectory from **4 → 5**, which remains in the doublet spin state with only one unpaired electron.

Note that, unlike the initial rate-limiting hydrogen abstraction, for this reaction barrier the final state is significantly lower in energy than the transition state. This is because the radical species remaining after hydrogen abstraction is significantly stabilized by the bonding to oxygen and molybdenum that allows for significantly more electron delocalization that is possible across only the three carbon atoms of the free allyl radical. Reoxidation of the H abstraction site in **5** produces structure **6**, which still has electron delocalization across the entire acrolein fragment resulting in partial order bonds (see bond distances in Table 2).

In Structure **7**, the product has disassociated from the molybdenum to generate adsorbed acrolein with a fully formed carbon-oxygen double bond and a reduced $Mo^{4+}=O$ site. Acrolein adsorbs quite favorably at Bi^{3+} cations via donation of electron density from one of the lone pairs on oxygen to the under-coordinated bismuth cation. Note that **6 → 7** requires substantial rearrangement of the oxygen atoms around molybdenum, which is in a triplet state with an unpaired electron in each of two distinct d orbitals. Formation of **7** is

energetically uphill, and may be facilitated by simultaneous molecular oxygen adsorption on the molybdenum, as suggested by Goddard *et al.*;[23] however we find that interaction with O_2 is not required for reasonable reaction energies. The oxygen vacancy in **7** created upon acrolein formation is then restored by atomic oxygen to form Structure **8**; however, we did not attempt to elucidate the details of this process. As observed in Fig. 2, this step is extremely favorable thermodynamically.

Table 2. Bond distances and formal bond orders (*B.O.*) from optimized structures **3-8**.

| Structure #	Mo–O distance (Å)	O–C_1 distance (Å)	C_1–C_2 distance (Å)	C_2–C_3 distance (Å)
3	1.74 *B.O. = 2*	*No bond*	1.38 *B.O. = 1.5*	1.37 *B.O. = 1.5*
4	2.00 *B.O. = 1*	1.41 *B.O. = 1*	1.49 *B.O. = 1*	1.33 *B.O. = 2*
5	2.02 *B.O. = 1*	1.30 *B.O. = 1.5*	1.36 *B.O. = 1.5*	1.40 *B.O. = 1.5*
6	2.03 *B.O. = 1*	1.28 *B.O. = 1.5*	1.41 *B.O. = 1.5*	1.35 *B.O. = 1.5*
7 & 8	*No bond*	1.21 *B.O. = 2*	1.45 *B.O. = 1*	1.33 *B.O. = 2*

The final step in propene oxidation is desorption of acrolein from the catalyst surface, thereby regenerating the bare surface (**0**). As mentioned in Section 3.3, acrolein has a C-H bond that is likely just slightly stronger than what can easily be broken by $Bi_2Mo_3O_{12}$, and is therefore reasonably stable to subsequent oxidation. We do observe high conversion of acrolein and ammonia to acrylonitrile (see Section 3.7), but this reaction must be facilitated by ammonia, since acrolein is not observed to undergo additional reaction at 673 K over $Bi_2Mo_3O_{12}$ without ammonia present.[4]

3.5 Propene Ammoxidation to Acrylonitrile

Scheme 1 shows the pathway for propene oxidation to acrolein in the presence of a spectator ammonia molecule (structure numbers are the numbers for the same structure without ammonia followed by an "N"). The energies for this pathway are shown in Fig. 5 so that they can be compared with those for the propene ammoxidation to acrylonitrile pathway shown in Scheme 2. In agreement with experiment, and as already discussed in Section 3.4, the activation of propene to produce allyl radical (steps **0 → 3**, see Fig. 2) is common to all product pathways.[9,20]

As proposed in our recent experimental work, we hypothesize that C-N bonds are formed by reaction of allyl alkoxide species with adsorbed ammonia.[4] Ammonia adsorbs favorably on surface Bi^{3+} cations via sigma donation of electron density from the lone pair on nitrogen to empty bismuth orbitals. Using our periodic $Bi_8Mo_{12}O_{48}$ slab model, we calculate the energy of ammonia adsorption over Bi^{3+} to be -17.9 kcal/mol on a fully oxidized surface. Since the orbitals of bismuth are very large and diffuse, ammonia can be anywhere in a ~2Åx2Å area, as long as the nitrogen lone pair points toward a Bi^{3+} that is 2.6-3.0Å away, and have approximately the same energy of adsorption. We find that adsorption of ammonia next to an adsorbed allyl (**3 → 3N**) is essentially equivalent to ammonia adsorption on a bare catalyst surface (-17.2 vs. -17.9 kcal/mol).
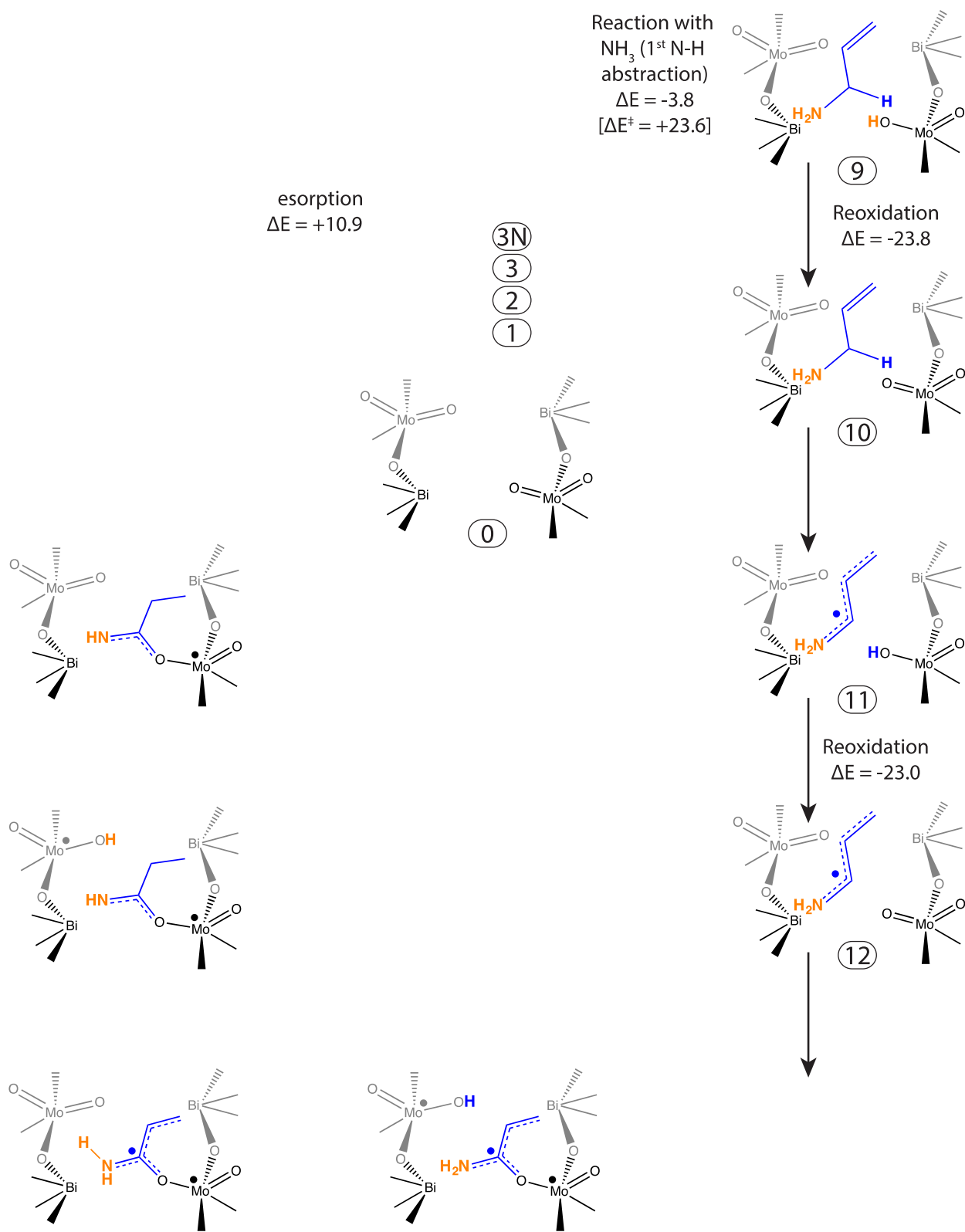
Scheme 2. Proposed elementary steps for propene ammoxidation to acrylonitrile (ΔE in kcal/mol).
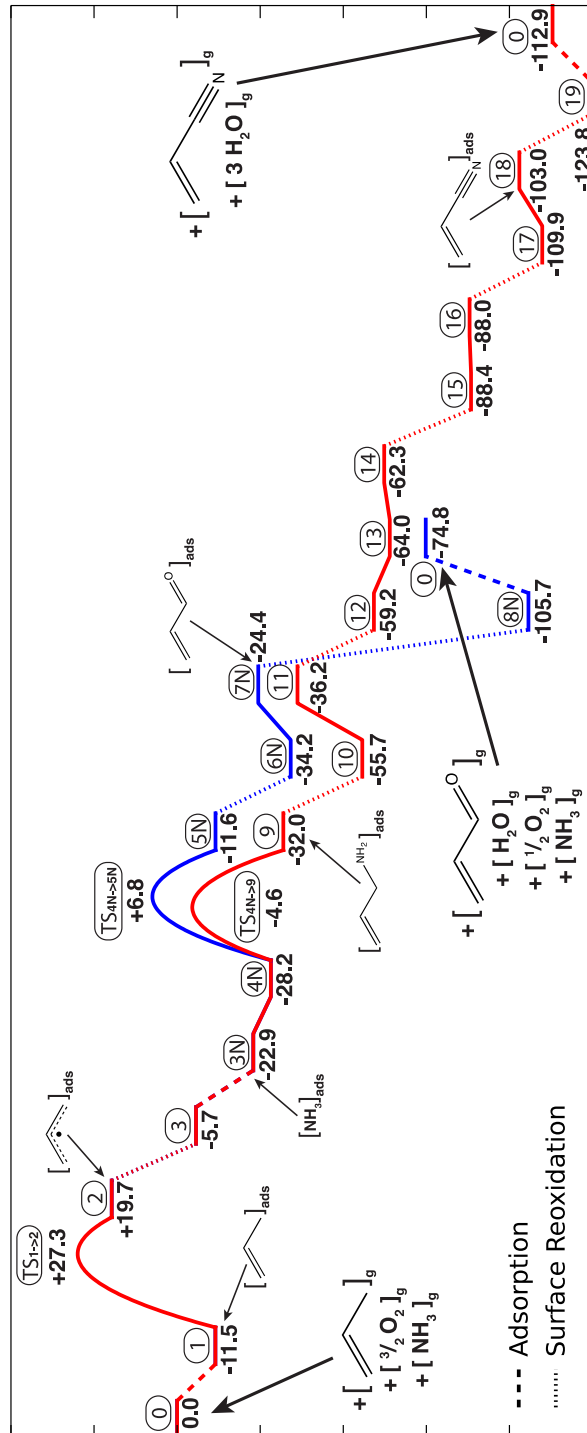
Fig. 5 Energy landscape for propene ammoxidation to acrylonitrile. Encircled integers refer to structures in Scheme 2, bold numbers give the energy of each structure relative to the initial state.

We propose that reaction of allyl alkoxide species with adsorbed ammonia in structure **4N** produces allylamine, which then undergoes further reaction to form acrylonitrile (or acetonitrile and HCN). In the schemes, we indicate that ammonia adsorbs on structure **3** to form **3N**, which then undergoes allyl insertion to form **4N**; however, ammonia could just as easily adsorb after insertion to form **4N** directly from **4** or could already be present before the allyl radical is formed. We note that while we indicate that ammonia is adsorbed on the Bi^{3+} cation that perturbs the allyl alkoxide oxygen, ammonia could also adsorb on either of the two neighboring Bi^{3+} sites to either side of the allyl alkoxide species, since they are also close enough to allow reaction between the ammonia and the allyl alkoxide species.

The allyl alkoxide intermediate (**4N**) can undergo one of two competing processes – abstraction of an H atom to form adsorbed acrolein and a neighboring Mo-OH group (**5N**) or reaction with adsorbed ammonia to form adsorbed allylamine and a Mo-OH group (**9**). The activation barrier for **4 → 5** was discussed in detail in Section 3.4 (see Fig. 4). We did not recalculate the activation barrier when a spectator ammonia molecule in adsorbed, but as can be seen by comparing the left- and right-hand sides of Scheme 1, the presence of a spectator ammonia does not have a significant effect on the values of $\Delta E_{reaction}$. Since the adsorbed ammonia does not lie along the **4 → 5** reaction pathway, but rather is situated off to the side, its presence should not affect the reaction barrier and therefore we assumed that ΔE_{TS} for **4N → 5N** is the same as for **4 → 5**.

Our calculated potential energy for reaction of the allyl alkoxide species with ammonia to form allylamine is shown in Fig. 6. We found ΔE_{TS} to be 23.6 kcal/mol and $\Delta E_{reaction}$ to be -3.8 kcal/mol. The initial movement along the reaction pathway involves

detachment of the allyl species, converting **4N** back to **3N**, so that the allyl species in **3N** is favorably adsorbed above the bismuth cation. This part of the pathway accounts for the section of the reaction coordinate between 0 Å and 5 Å in Fig. 6. We found that the interaction between allyl and bismuth cation leads to a significantly lower reaction barrier than for the same pathway in which the allyl radical is further above the surface and thus not able to interact with the bismuth cation. The transition state for reaction **4N → 9** is the umbrella flip of ammonia, which removes the favorable lone pair interaction with the surface bismuth cation and forms a less favorable interaction with the electrophilic carbon of the allyl species. After the ammonia inverts, formation of the C-N bond followed by loss of a hydrogen atom to a surface molybdenyl oxo to form allylamine is highly exothermic. This reaction is a nucleophilic substitution reaction that most likely occurs by interaction of ammonia with an allyl cation to form allyl-NH_3^+ that then loses a proton to the oxygen anion to form allylamine. Once the allyl-NH_3^+ species loses a proton to the molybdenyl oxo, the nitrogen of allylamine can reform the favorable interaction with the surface bismuth cation that was lost in the transition state. The allylamine formed in reaction **4N → 9** has the lowest adsorption energy of any species we investigated (ΔE_{ads} = -23.7 kcal/mol) because it has favorable, dative-type interactions from both the nitrogen lone pair and the carbon-carbon pi bond to two neighboring bismuth cations.

Overall, the activation barrier for allylamine formation is reasonably low because ammonia is stabilized by interaction with the carbon atom of the allyl species before it loses a hydrogen atom. As can be seen in Table 1, the N-H bonds of ammonia are significantly stronger than the C-H bond of the methyl group of propene that is broken in the rate-limiting step. We examined alternative pathways for the interaction of ammonia with various

hydrocarbon intermediate species, but found that, because of the high bond dissociation energy of the N-H bonds of NH_3, any reaction step that began with abstraction of an H atom from ammonia was not favorable. From this we conclude that ammonia can only be activated by $Bi_2Mo_3O_{12}$ once the nitrogen fragment that will be formed upon hydrogen abstraction is first stabilized by favorable interaction with either the catalyst surface or a hydrocarbon species.
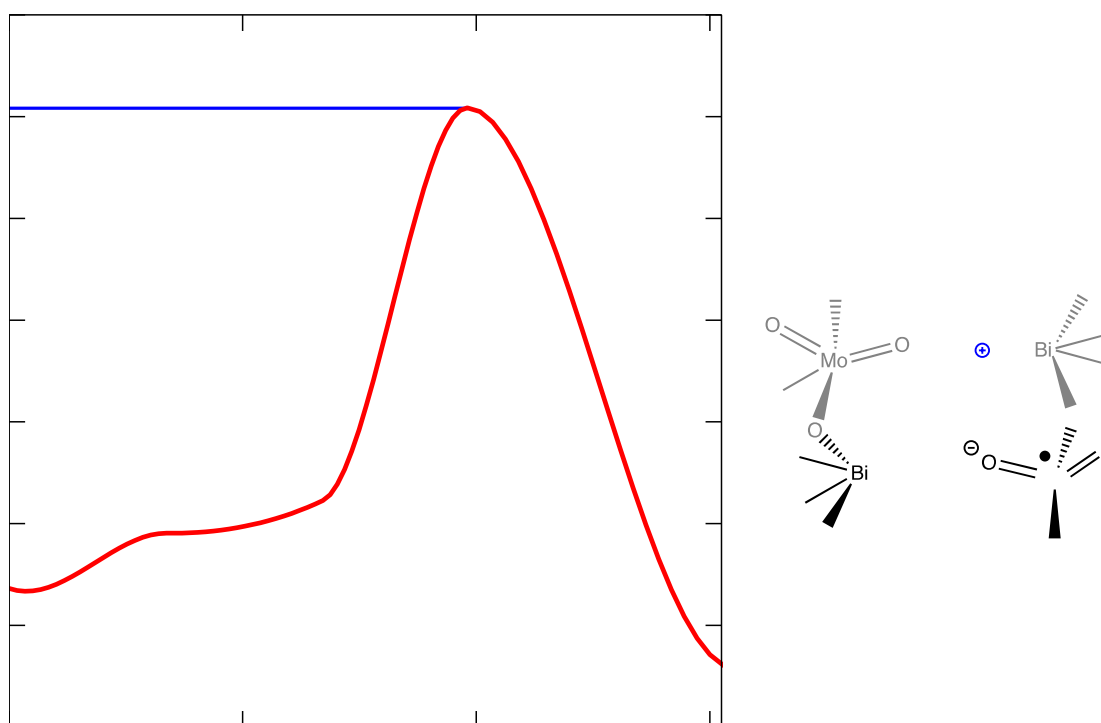

Fig. 6 Reaction barrier for reaction of allyl alkoxide and ammonia to produce adsorbed allylamine, with relevant energies annotated. Geometries for the initial state (A), transition state (B) and final state (C) are shown on the right, with relevant distances in Å indicated.

Comparing the reaction barrier of **4N → 9** with **4N → 5N**, it is clear that production of allylamine is energetically favored by more than 10 kcal/mol over production of acrolein when a neighboring ammonia molecule is present. The transition state for allylamine

formation is also likely to be entropically favored over the transition state for acrolein formation, since the former has two separate physisorbed molecules that have not yet come together, whereas the later is very geometrically-constrained. Therefore, at reaction temperatures, if an ammonia molecule adsorbs at any of the three bismuth cations near an allyl alkoxide species, allylamine will always be produced. However, acrolein can still be formed via reaction **4 → 5** if ammonia is not adsorbed nearby. The ratio of acrylonitrile to acrolein is therefore only dependent on the ammonia adsorption, which is a function of ammonia partial pressure to the first order in this low coverage regime. Experimentally, we have observed that the ratio of acrylonitrile to acrolein is approximately first order in ammonia partial pressure and we have estimated that the activation barrier for acrolein formation is ~15 kcal/mol higher than the barrier height for acrylonitrile formation at the same stage in the reaction sequence.[4] In summary, our DFT calculations for steps **4N → 5N** and **4N → 9** are consistent with the difference in the activation energies that we determined from analysis of the reaction kinetics.

As discussed in Section 3.2, once H atoms are abstracted from a reacting species onto the catalyst surface, the catalyst is reoxidized, e.g., step **9 → 10 11 → 12**, **14 → 15**, **16 → 17**, and **18 → 19** (all indicated in Fig. 5 by hashed lines). These steps provide the thermodynamic driving force for all reactions involving the cleavage of C-H or N-H bonds.

Allylamine has two relatively weak C-H bonds (see Table 1 for BDEs), and should thus undergo facile hydrogen abstraction. Note that, since allylamine adsorbs quite strongly on the surface of $Bi_2Mo_3O_{12}$ via favorable electron donation from the nitrogen and from the carbon-carbon double bond to neighboring Bi^{3+} cations, it is unlikely to escape the reactor intact. Experimentally, we have observed a high conversion of allylamine when it is fed to

the reactor under conditions where propene would only exhibit differential conversion and consequently we are not able to observe any allylamine during propene ammoxidation.[4] The allyl–NH_2 radical species formed by abstracting one of these H atoms (Structure **11**) is significantly more stable than the allyl species formed in the rate-limiting step, since resonance structures involving both the lone pair on the nitrogen atom and the carbon-carbon pi bond electrons stabilize the radical. It is evident from the bond distances given in Table 3 that the radical is delocalized across the entire fragment, resulting in all C-C and C-N bonds being 1.5 order.

Estimates of the activation barrier for reaction **10 → 11** suggest that this reaction has a singlet-triplet spin crossing transition state that is only a few kcal/mol higher in energy than the final state. A transition-state energy similar to the final-state energy is also observed for the initial hydrogen abstraction from propene (see above). Therefore, because of high computational demand needed to determine any singlet-triplet crossing transition state, this reaction barrier was not fully optimized. However, since the difference between the transition state and the final state in the rate-limiting hydrogen abstraction from propene (step **1 → 2**) is only 7.6 kcal/mol, we expect that the very similar reaction of **10 → 11** has a transition state of ≤8 kcal/mol above the final state. Consequently, the activation of allylamine should be significantly less demanding (by approximately the 11.7 kcal/mol difference in their values of ΔE_{rxn}) than the activation of propene, and therefore will occur easily and not affect the overall rate of propene conversion.

We hypothesized initially that after formation of the allyl-NH_2 radical (**10 → 11**) and reoxidation of the catalyst surface (**11 → 12**), one of the H atoms from the NH_2 group would be abstracted to form 2-propen-1-imine ($NH=CH-CH=CH_2$), a compound similar to acrolein.

However, all attempts to react this species over our model surface resulted in very high values of $\Delta E_{reaction}$, due to the absence of any weak C-H or N-H bonds (see Table 1). We therefore considered an alternate mechanism, in which the allyl-NH_2 radical is first stabilized by insertion into a surface molybdenum-oxygen double bond (**12 → 13**), thereby facilitating subsequent reactions. This reaction is the same as step **3 → 4** in the pathway for propene oxidation, except that the allyl species has a terminal -CH-NH_2 group instead of a terminal -CH_2 group. As can be seen in Table 3, reaction of the allyl-NH_2 fragment with a surface Mo=O group generates all integer bonds.

The remaining alpha C-H bond of **13** is still quite weak (see Table 1, approximated by 2-propen-1-ol-1-amine) and consequently its abstraction in step **13 → 14** is close to thermoneutral. The resulting tertiary carbon radical is highly stabilized by conjugation. The electron delocalization across the nitrogen, primary carbon and oxygen atoms results in a lengthening of the molybdenum-oxygen distance such that it is no longer a single bond. Interestingly, despite the possible resonance structures involving the carbon-carbon double bond, the bond distances listed in Table 3 indicate that substantial electron delocalization only occurs among the nitrogen, primary carbon, and oxygen atoms. The -ene group appears to be nearly completely formed, likely because the electron-withdrawing nitrogen and oxygen atoms are sufficient to stabilize the carbon radical. This step completes the necessary removal of the three H atoms from the methyl group of propene.

After reoxidation (**14 → 15**), abstraction of one of the equivalent H atoms from the terminal NH_2 group occurs via another essentially thermoneutral process to form **16**. As mentioned above and indicated in Table 1, N-H bonds are generally very high in energy and thus difficult to break. However, a hydrogen atom can easily be abstracted from **16**, because

doing so regenerates the lone pair on nitrogen as the bond count on that atom goes from 3.5 to 2.5. This step is then followed by another reoxidation to form structure **17.** The bond distances of Table 3 indicate that structures **16** and **17** have approximately 1.5 order bonds between the primary carbon and both nitrogen and oxygen, rather than the expected double bond to nitrogen and single bond to oxygen. These 1.5 order bonds to both nitrogen and oxygen are a result of both heteroatoms having lone pairs of electrons that can interact with the electrons on the primary carbon and the highly electrophilic oxygen pulling electron density from the -C=NH group.

Table 3. Bond distances and formal bond orders (*B.O.*) from optimized structures **10**-**19**.

Structure #	Mo–O distance (Å)	O–C_1 distance (Å)	C_1–N distance (Å)	C_1–C_2 distance (Å)	C_2–C_3 distance (Å)
10	1.75 *B.O. = 2*	*No bond*	1.48 *B.O. = 1*	1.49 *B.O. = 1*	1.32 *B.O. = 2*
11 & 12	2.01 *B.O. = 1*	*No bond*	1.35 *B.O. = 1.5*	1.39 *B.O. = 1.5*	1.36 *B.O. = 1.5*
13	2.01 *B.O. = 1*	1.39 *B.O. = 1*	1.47 *B.O. = 1*	1.50 *B.O. = 1*	1.32 *B.O. = 2*
14 & 15	2.17 *B.O. = 0.5*	1.25 *B.O. = 1.5*	1.33 *B.O. = 1.5*	1.46 *B.O. = 1*	1.33 *B.O. = 2*
16 & 17	2.05 *B.O. = 1*	1.29 *B.O. = 1.5*	1.30 *B.O. = 1.5*	1.47 *B.O. = 1*	1.33 *B.O. = 2*
18 & 19	1.75 *B.O. = 2*	*No bond*	1.17 *B.O. = 3*	1.42 *B.O. = 1*	1.34 *B.O. = 2*

Again, the final N-H bond in **17** is reasonably strong and could likely not be broken on its own (see Table 1, approximated by 2-propen-1-ol-1-imine). However, because this last hydrogen removal can be coupled with breaking the carbon-oxygen bond to release the acrylonitrile product, it still has a reasonable energy (**17 → 18**). Despite being mildly endothermic, this reaction will be favored entropically, since it releases a physisorbed

product from a bound intermediate. Catalyst reoxidation (**18 → 19**) and desorption of acrylonitrile (**19 → 0**) completes the catalytic cycle, producing in total 1 acrylonitrile and 3 water molecules from 1 propene, 1 ammonia and $^3/_2$ oxygen molecules. Since acrylonitrile does not have any weak C-H bonds to attack, it should be stable to further oxidation, which is what is observed when acrylonitrile is fed over the catalyst at standard reaction conditions.[4]

3.6 Formation of Acetonitrile and Hydrogen Cyanide

Our experimental work has shown that acetonitrile (CH_3CN) and hydrogen cyanide (HCN) are intrinsic products produced directly from propene, and not via secondary reactions involving either acrolein or acrylonitrile.[4] Given that allylamine is a likely intermediate on the pathway from propene and acrylonitrile and that ammoxidation of allylamine produces a similar ratio of byproducts to acrylonitrile as does ammoxidation of propene, we hypothesized that allylamine might also react to form CH_3CN and HCN. Since the byproducts have a higher N/C ratio than acrylonitrile and increasing the partial pressure of ammonia increases the selectivity to these byproducts,[4] we further hypothesized that allylamine might react with another ammonia molecule to form a 2C-1N fragment and a 1C-1N intermediate that could undergo additional reaction to form CH_3CN and HCN, respectively. Our experimental work showed that 1,2-diaminopropane, the product of direct Markovnikov addition of ammonia across the carbon-carbon double bond of allylamine, did not react over the catalyst under the conditions used for propene ammoxidation.[4] We note, however, that the C-C bond of 1,2-diaminopropane is very weak (BDE = 77.6 kcal/mol), suggesting that if a similar species, but one stabilized by interaction with the catalyst, could form, it might serve as an intermediate to lower carbon number products. An illustration of

this idea has already been discussed in Sections 3.4 and 3.5, where it was shown that intermediates stabilized by insertion into Mo=O bonds facilitated transformations that could not occur in the gas phase. As discussed below, we found that a species derived from allylamine bound to a surface molybdenyl oxo (Structure **13**), could react to form CH_3CN and HCN via an energetically plausible pathway.

The formation of CH_3CH and HCN begins with allylamine adsorption onto a bare catalyst surface (Structure **10**), and then continues via steps **10 → 11 → 12 → 13** shown in Scheme 2. The subsequent steps leading to the two byproducts are shown in Scheme 3. As indicated in Fig. 7, the adsorption of ammonia at a nearby Bi^{3+} cation produces structure **13N**. The adsorption is favorable, though not as favorable as on a bare surface; this is likely an artifact of artificial repulsive interactions between the two adsorbed molecules in neighboring unit cells, a consequence of the periodic boundary conditions.
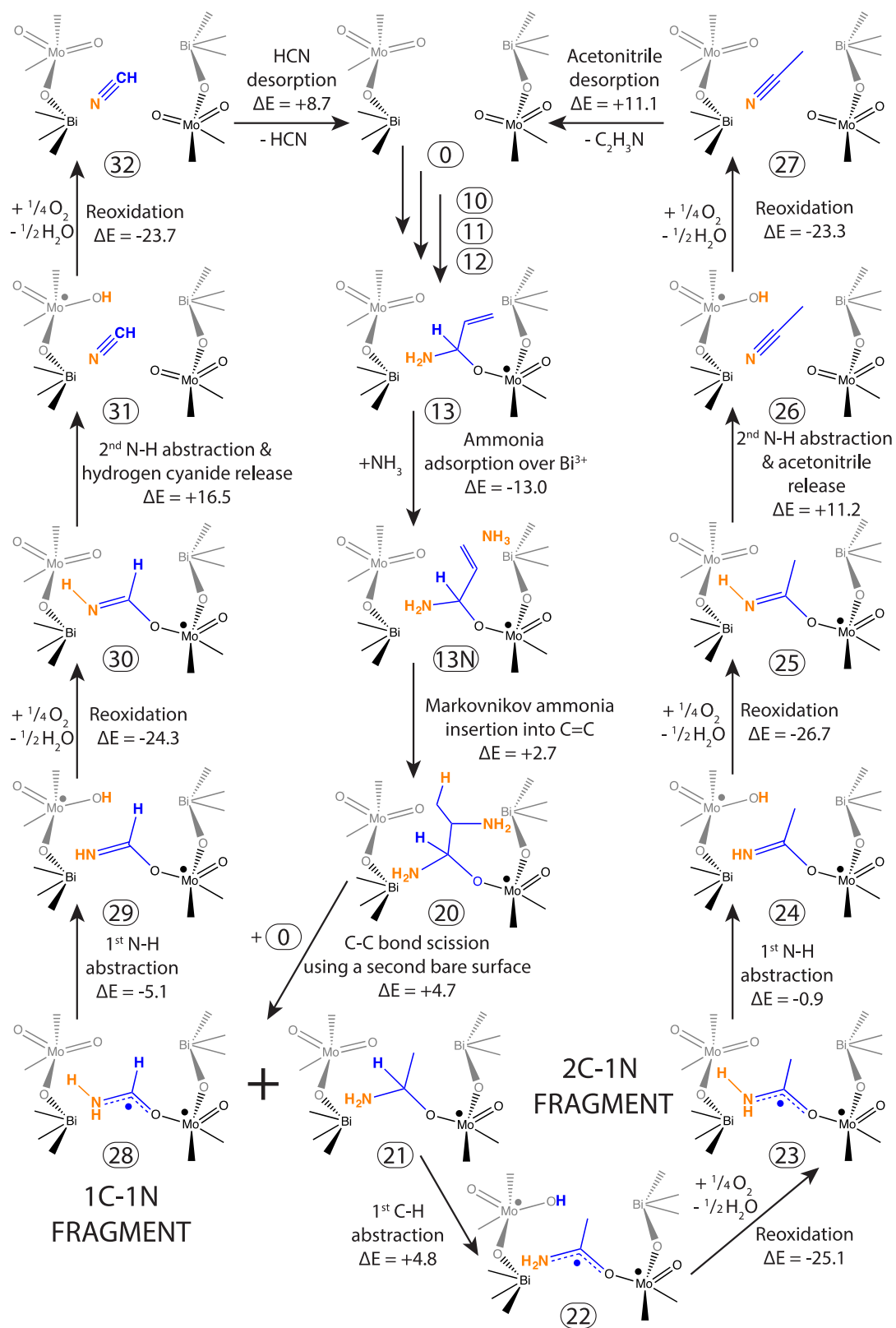
Scheme 3. Proposed elementary steps for allylamime ammoxidation to acetonitrile and hydrogen cyanide (ΔE in kcal/mol).
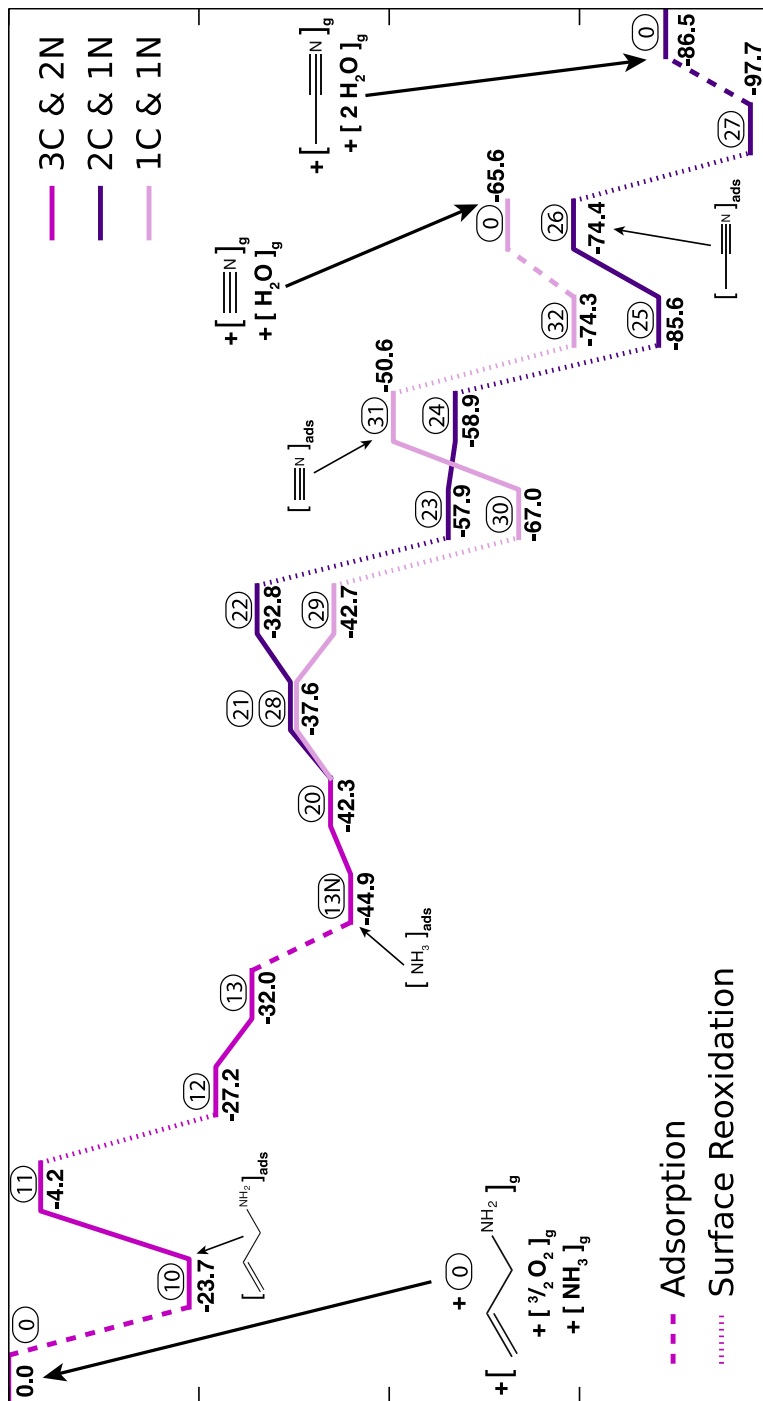
Fig. 7 Energy landscape for allylamine ammoxidation to acetonitrile and hydrogen cyanide. Encircled integers refer to structures in Scheme 3, bold numbers give the energy of each structure relative to the initial state.

The Markovnikov addition of adsorbed ammonia across the carbon-carbon double bond of **13N** gives structure **20**. This reaction is actually only very slightly uphill in energy. Breaking the C-C bond between the two carbon atoms that are each bound to nitrogen would result in a 2C-1N fragment that could become CH_3CN and a 1C-1N fragment that could become HCN. We hypothesize that this C-C bond cleavage reaction involves a nearby $O=Mo^{6+}=O$ moiety to abstract the 2C-1N fragment, leaving behind the 1C-1N fragment. Because of the constraints of the periodic unit cell, we found that accommodation of both fragments in one calculation resulted in a very high reaction energy ($\Delta E_{rxn} > +25$ kcal/mol). However, the energy difference of **20** plus a bare surface **0** and a surface with the bound 2C-1N fragment (**21**) plus a surface with the bound 1C-1N surface (**28**) is only $\Delta E_{rxn} = +6.7$ kcal/mol. While we expect some minor repulsive interaction between fragments on two neighboring molybdenum sites, it is not realistic for this interaction to be so high in energy. Therefore, we believe that the high ΔE_{rxn} structure is unphysical and is a consequence of the highly repulsive interactions between fragments in neighboring unit cells. On the actual catalyst surface, the 2C-1N fragment could be abstracted by a neighboring $O=Mo^{6+}=O$ site and easily rotate to be far enough away from the remaining 1C-1N fragment so as to not interact substantially. Therefore, while we are not able to calculate the reaction barrier for C-C bond cleavage, our approximation of the energy of reaction indicates that this reaction is likely to be feasible, since the reaction energy is only 4.7 kcal/mol and the reaction entropy is negative. The low reaction energy is due, in part, to the low bond energy of the C-C bond in **20** (80.1 kcal/mol) relative to that in adsorbed allylamine (96.1 kcal/mol) resulting from the presence of the second amine group in **20**. We note further that rate of reaction **13N** → **20**, and hence **20** → **21** + **28**, depends on the surface coverage of adsorbed NH_3, which

decreases with decreasing ammonia partial pressure. This projection is fully consistent with our experimental findings.[4]

Following C-C cleavage, the two fragments produced in step (**20 + 0**) → (**21 + 28**) follow independent trajectories to their respective final products, CH_3CN and HCN. The 2C-1N fragment progresses through structures **21** through **27**, whereas the 1C-1N fragment progresses through structures **28** through **32**. To illustrate these reactions on the energy landscape shown in Fig. 7, we simply used the sum of the energies of structures **21** and **28** as the starting point, and then added or subtracted the energy difference between each structure and structure **21** (CH_3CN pathway) or **28** (HCN pathway) for the remaining steps. The steps are very similar to each other and follow the same trends with BDE as discussed in detail above for propene ammoxidation to acrylonitrile; therefore, they do not require much discussion beyond the fact that they are energetically favorable. Bond distances for all optimized structures **20** through **32** are presented in Table 4.

We propose that the first reaction of the 2C-1N fragment is a hydrogen atom abstraction from the central carbon to give **22**, since this bond is significantly weakened by the surrounding electron withdrawing O-Mo and NH_2 groups. This reaction is endothermic, but the energy is quite low for a hydrogen abstraction step. As in structure **14** discussed above, there is substantial electron delocalization between the nitrogen, primary carbon and oxygen atoms, such that each of those bonds is ~1.5 order, which results in the Mo-O bond order being less than 1. After the requisite reoxidation to give **23**, the fragment can lose one of the H atoms on the NH_2 group to leave a stable C=NH moiety (Structure **24**), a process that is energetically favorable. After reoxidation to give structure **25**, the resulting fragment can lose its final H atom to a neighboring site and desorb from the catalyst surface (Structure

26). This final step is energetically uphill, but will be entropically favorable, since a physisorbed acetonitrile is produced from a bound species. A final reoxidation step to give **27** and finally desorption of the favorably adsorbed acetonitrile completes the catalytic cycle for a highly thermodynamically favorable reaction.

The reactions of the 1C-1N fragment are very similar to those of the 2C-1N fragment; however, because the fragment resulting from the C-C scission is a radical, the initial H abstraction from the NH_2 group to give Structure **29** is exothermic. After surface reoxidation, the fragment loses its final H atom and releases HCN from the surface (Structure **31**) in an energetically unfavorable, but entropically favorable, step. Reoxidation of the catalyst to give **32** and gas-phase HCN regenerates the bare surface in another highly exothermic reaction.

Table 4. Bond distances and formal bond orders (*B.O.*) from optimized structures **20-32**.

Structure #	$Mo_1–O_1$ or $Mo_2–O_2$ distance (Å)	$O_1–C_1$ or $O_2–C_2$ distance (Å)	$C_1–N_1$ or $C_2–N_2$ distance (Å)	$C_1–C_2$ or $C_2–C_3$ distance (Å)
20	2.01 [$Mo_1–O_1$] *B.O. = 1*	1.40 [$O–C_1$] *B.O. = 1*	1.45 [$C_1–N_1$] *B.O. = 1* 1.47 [$C_2–N_2$] *B.O. = 1*	1.56 [$C_1–C_2$] *B.O. = 1* 1.52 [$C_2–C_3$] *B.O. = 1*
21	2.00 [$Mo_2–O_2$] *B.O. = 1*	1.42 [$O_2–C_2$] *B.O. = 1*	1.48 [$C_2–N_2$] *B.O. = 1*	1.50 [$C_2–C_3$] *B.O. = 1*
22 & 23	2.17 [$Mo_2–O_2$] *B.O. = 0.5*	1.25 [$O_2–C_2$] *B.O. = 1.5*	1.33 [$C_2–N_2$] *B.O. = 1.5*	1.49 [$C_2–C_3$] *B.O. = 1*
24 & 25	2.05 [$Mo_2–O_2$] *B.O. = 1*	1.30 [$O_2–C_2$] *B.O. = 1.5*	1.30 [$C_2–N_2$] *B.O. = 1.5*	1.50 [$C_2–C_3$] *B.O. = 1*
26 & 27	1.74 [$Mo_2–O_2$] *B.O. = 2*	*No bond*	1.15 [$C_2–N_2$] *B.O. = 3*	1.43 [$C_2–C_3$] *B.O. = 1*
28	2.17 [$Mo_1–O_1$] *B.O. = 0.5*	1.25 [$O_1–C_1$] *B.O. = 1.5*	1.32 [$C_1–N_1$] *B.O. = 1.5*	
29 & 30	2.05 [$Mo_1–O_1$] *B.O. = 1*	1.29 [$O_1–C_1$] *B.O. = 1.5*	1.29 [$C_1–N_1$] *B.O. = 1.5*	
31 & 32	1.74 [$Mo_1–O_1$] *B.O. = 2*	*No bond*	1.15 [$C_1–N_1$] *B.O. = 3*	

Both acetonitrile and HCN are stable products, consistent with the high BDEs for the remaining hydrogen atoms (Table 1).[4] However, we do observe experimentally that HCN and acetonitrile are produced in the constant ratio of approximately 5 HCN: 2 acetonitrile. Therefore, one third of the 2C-1N intermediates reacts with another ammonia to make two 1C-1N fragments that both become HCN. The most likely scenario for this reaction is attack of the electron-deficient primary carbon of **25** by the lone pair on nitrogen, before **25** undergoes the endothermic final hydrogen abstraction and acetonitrile release to form **26**.
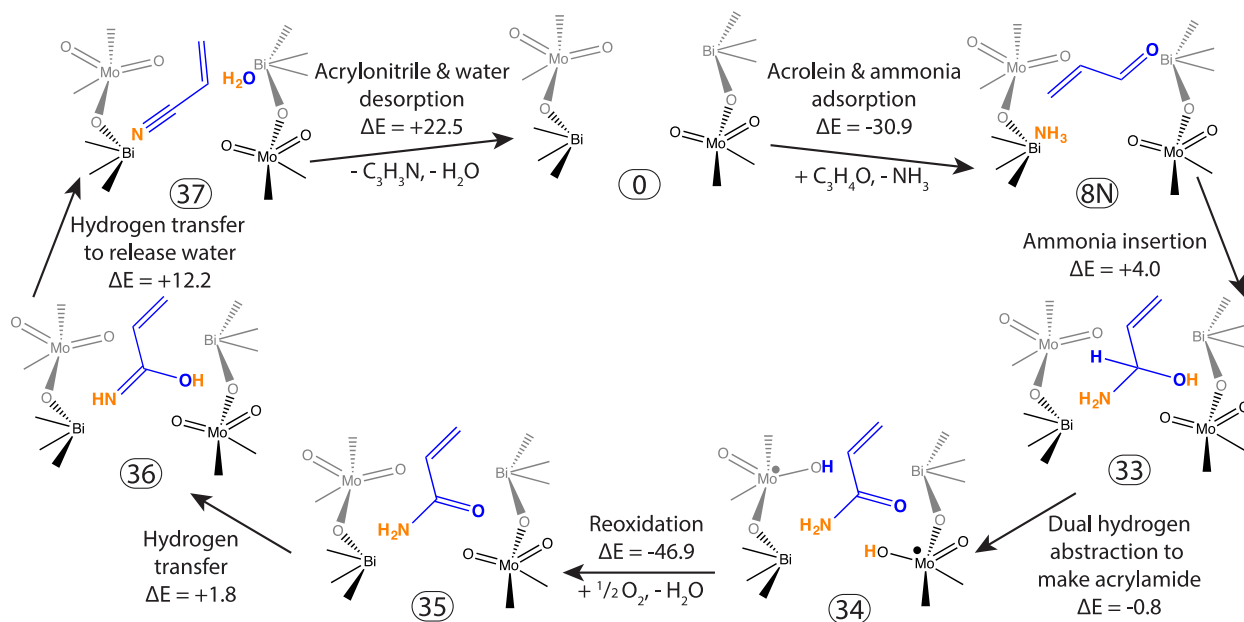
3.7 Acrolein ammoxidation to acrylonitrile

The final reaction we investigated is acrolein ammoxidation to acrylonitrile, which has been reported to be both facile over bismuth molybdate but of minor importance, accounting for less than about 10% of the acrylonitrile formed from propene.[4,5,8] Our proposed mechanism for this reaction is shown in Fig. 8. This pathway does not follow the same trends as the other pathways discussed above, as transformations occur mostly between adsorbed molecules and the catalyst only serves to stabilize the species and to perform one hydrogen abstraction step in the pathway. However, it is the only chemically and energetically reasonable set of elementary steps that we were able to discover for this reaction that experimentally has a very low activation energy of ~7kcal/mol[8].

The first step in this reaction (**0 → 8N**) involves adsorption of ammonia and acrolein, both of which occur favorably over Bi^{3+} cations via donation from lone pairs on the respective heteroatoms. These molecules are adsorbed on neighboring Bi^{3+} atoms that are 5 Å apart. Note that **8N** is the structure formed at the end of the pathway leading to acrolein in

the presence of a spectator ammonia. Therefore, acrolein formed along that pathway could react immediately with an adsorbed ammonia molecule to form acrylonitrile rather than desorbing.

The next step is addition of ammonia across the carbon-oxygen double bond of acrolein (**8N → 33**). We note that, according to gas phase calculations, addition across this double bond is not as favorable as Markovnikov addition across the carbon-carbon double bond, as is done for allylamine conversion to acetonitrile and HCN (for NH_3 addition across C=O bond, ΔE = -8.1 kcal/mol; for NH_3 addition across the C=C bond, ΔE = -17.4 kcal/mol). However, addition across the carbon-carbon double bond leaves an NH_2 bound to the central carbon and one terminal methyl group, so it is difficult to imagine how this species could become acrylonitrile, and, experimentally, acrolein converts almost completely to acrylonitrile in the presence of ammonia[4]. We also considered other pathways for the reaction of acrolein, including one beginning with the abstraction of the reasonably high BDE aldehyde hydrogen ($\Delta E_{reaction}$ ~30 kcal/mol) and another in which acrolein inserts into a molybdenyl oxygen at the primary carbon atom ($\Delta E_{reaction}$ ~50 kcal/mol). However, because of the high energies associated with these alternatives, neither is feasible for this low energy reaction.

Scheme 4. Proposed elementary steps for acrolein ammoxidation to acrylonitrile (ΔE in kcal/mol).
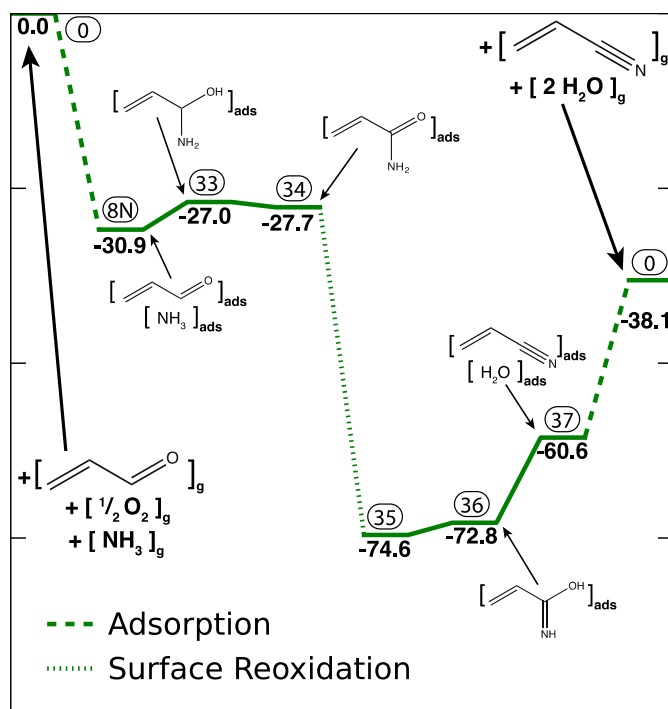

Fig. 8 Energy landscape for acrolein ammoxidation to acrylonitrile. Encircled integers refer to structures in Scheme 4, bold numbers give the energy of each structure relative to the initial state.

The addition of ammonia across the carbon-oxygen double bond of acrolein to form **33** is entropically disfavored and has a significant positive free energy in the gas phase (ΔG_{673K} = +20.1 kcal/mol). However, both acrolein and ammonia adsorb quite favorably on the surface of bismuth molybdate, promoting the reaction of the adsorbed molecules by increasing the probability of their interaction and thereby reducing the entropy loss of their combination compared to that for reaction in the gas phase. This initial addition of ammonia to acrylonitrile (**8N → 33**) is likely to be the rate-limiting step for this reaction, since it is at the beginning of the pathway and both is mildly energetically and entropically disfavored.

The next step in this reaction is the sequential abstraction of two hydrogen atoms from **33** to form **34**. We initially tried to abstract only the hydrogen on the highly-substituted alpha carbon, since this bond is very weak (see Table 1, 2-propen-1-ol-1-amine); however, during optimization, the radical also shed the hydroxyl hydrogen onto a nearby molybdenyl oxo to create a charge neutral acrylamide. Favorable reoxidation with ½ O_2 removes both surface hydrogen atoms, leaving the adsorbed acrylamide (**35**).

Reaction of acrylamide to acrylonitrile and water involves two internal hydrogen atom transfers from the NH_2 group of acrylamide to the oxo group (**35 → 36 → 37**), followed by desorption. The internal hydrogen transfers of the adsorbed molecule may occur on their own or be facilitated by catalyst surface oxygen atoms. Considering the energy pathway in Fig. 8, this reaction appears to be energetically unfavorable. Gas-phase calculations also show that this reaction is quite unfavorable at 0 K (ΔE = +26.0 kcal/mol) but at reaction temperature, (673 K) it becomes favorable (ΔG_{673K} = -4.4 kcal/mol). The likelihood of acrylamide as an intermediate in the formation of acrylonitrile is also supported by experimental observation. We tested the reaction of acrylamide in the presence of water

vapor and oxygen over bismuth molybdate at 673 K, and observed almost complete conversion to acrylonitrile (see Ref. 4 for details of the experimental setup). Therefore, despite the mildly unfavorable energetics of Fig. 8, a pathway from acrolein to acrylonitrile via acrylamide appears to be feasible.

4. Conclusions

We have analyzed the energetics of propene oxidation and ammoxidation occurring on the (010) surface of $Bi_2Mo_3O_{12}$ with the objective of establishing whether the proposed reaction sequence suggested by our experimental studies[4] is energetically feasible. We find that the most energetically demanding reaction is activation of a C-H bond of a methyl group in propene and that this process occurs preferentially at bismuth-perturbed Mo=O groups on the catalyst surface via a singlet-to-triplet spin-state crossing that occurs with high probability due to favorable spin-orbit coupling. This reaction has an intrinsic activation barrier of 38.8 kcal/mol. Favorable propene adsorption, a consequence of electron donation from the carbon-carbon pi bond to under-coordinated surface bismuth cations, results in an apparent activation energy of 27.3 kcal/mol. The transition state for hydrogen abstraction is similar in both energy and geometry to the product state, a physisorbed allyl radical and a surface hydroxyl. Rapid and energetically favorable catalyst reoxidation accompanied by the release of water drives the activation reaction forward, offsetting the occurrence of the reverse reaction.

The allyl radical formed by propene activation is stabilized by reaction with a Mo=O group to form an allyl alkoxide. This species can then either undergo abstraction of its alpha hydrogen to form a surface-coordinated acrolein or reaction with NH_3 adsorbed via a dative

45

bond on a proximate Bi^{3+} cation to form allylamine. We show that the activation barrier for the latter process is significantly lower than for the former, consistent with the experimental observations that, in the presence of gas-phase ammonia, acrylonitrile is formed preferentially to acrolein, and that the selectivity to acrolein increases with increasing temperature.[4]

In agreement with our experimental results, our calculations confirm that allylamine is a viable intermediate on the pathway to acrylonitrile. Reaction of allylamine occurs by sequential abstraction of the four hydrogen atoms in order of increasing bond dissociation energy, with stabilization of the intermediate species via bonding with a surface molybdenyl oxo species. Reaction of a surface bound allylamine with a second molecule of adsorbed NH_3 leads to a diamine species containing a weak C-C bond that can undergo cleavage to form intermediates that after dehydrogenation produce CH_3CN and HCN. These findings are in good accord with experimental observation. Finally, we have shown that acrolein can be converted to acrylonitirile via a sequence of steps that likely involve the formation of acrylamide. While the latter intermediate has not been observed experimentally, the reaction of acrylamide is found to produce acrylonitrile with almost complete conversion in the presence of oxygen at 673 K over $Bi_2Mo_3O_{12}$.

5. Acknowledgements.

6. References

[1] Grasselli, R.K. *Top. Catal.* **2002**, *21*, 79-88.

[2] Arntz, D.; Fischer, A.; Höpp, M.; Jacobi, S.; Sauer, J.; Ohara, T.; Sato, T.; Shimizu, N.; Schwind, H. In *Ullmann's Encyclopedia of Industrial Chemistry*; Wiley-VCH: Weinheim, Germany, 2012.

[3] Brazdil, J.F. In *Ullmann's Encyclopedia of Industrial Chemistry*; Wiley-VCH: Weinheim, Germany, 2012.

[4] Licht, R.B.; Vogt, D.; Bell, A.T. *J. Catal.* **2016**, *339,* 228-241.

[5] Wragg, R.D.; Ashmore, P.G.; Hockey, J.A. *J. Catal.* **1973**, *31*, 293-303.

[6] Kolchin, I.K.; Bobkov, S.S.; Margolia, L.Y. *Neftekhimiya* **1964**, *4*, 301-307.

[7] Zhai, Z.; Getsoian, A.B.; Bell, A.T. J. *Catal.* **2013**, *308*, 25-36.

[8] Callahan, J.L.; Grasselli, R.K.; Milberger, E.C.; Strecker, H.A. *Ind. Eng. Chem. Prod. Res. Dev.* **1970**, *9*, 134-142.

[9] Adams, C.R.; Jennings, T.J. *J. Catal.* **1963**, *2*, 63-68.

[10] Adams, C.R.; Jennings, T.J. *J. Catal.* **1964**, *3*, 549-558.

[11] Krenze, L.D.; Keulks, G.W. *J. Catal.* **1980**, *61*, 316-325.

[12] McCain, C.C.; Gough, G.; Godin, G.W. *Nature* **1963**, *198*, 989-990.

[13] Burrington, J.D.; Kartisek, C.T.; Grasselli, R.K. *J. Org. Chem.* **1981**, *46*, 1877-1882.

14 Sachtler, W.M.H.; DeBoer, N.K. In *Proceedings 3rd International Congress on Catalysis*; 1965; Vol. 1, p 252.

15 Zhao, Y.; Truhlar, D.G. *J. Chem. Phys.* **2006**, *125* 194101-194118.

16 Getsoian, A.B.; Bell, A.T. *J. Phys. Chem. C*, **2013**, *117* 25562-25578.

17 Getsoian, A.B.; Shapovalov, V; Bell, A.T. *J. Phys. Chem. C* **2013**, *117* 7123-7137.

18 Haber, J.; Grzybowska, D. *J. Catal.* **1973**, *28*, 489-505.

19 Hanna, T.A. *Coord. Chem. Rev.* **2004**, *248*, 429-440.

20 Burrington, J.D.; Kartisek, C.T.; Grasselli, R.K. *J. Catal.* **1983**, *81*, 489-498.

21 Keulks, G.W. *J. Catal.* **1970**, *19*, 232-235.

22 Snyder, T.P.; Hill, C.G. *Catal. Rev.* **1989**, *31*, 43-95.

23 Pudar, S.; Oxgaard, J.; Chenoweth, K.; van Duin, A.C.T.; Goddard III, W.A. *J. Phys. Chem. C* **2007**, *111*, 16405-16415.

24 Burrington, J.D.; Kartisek, C.T.; Grasselli, R.K. *J. Catal.* **1984**, *87*, 363-380.

25 Pudar, S.; Oxgaard, J.; Goddard III, W.A. *J. Phys. Chem. C* **2010**, *114*, 15678-15694.

26 Jang, Y.H.; Goddard III, W.A. *J. Phys. Chem. B* **2002**, *106*, 5997-6013.

27 Kresse, G; Hafner, J. *Phys. Rev. B* **1993**, *47*, 558-561.

28 B Hammer, B.; Hansen, L.B.; Nørskov, J.K. *Phys. Rev. B* **1999**, *59*, 7413-7421.

29 Kresse, G.; Furthmüller, J. *Phys. Rev. B* **1996**, *54*, 11169-11186.

30 Blochl, P.E. *Phys. Rev. B* **1994**, *50*, 17953-17979.

31 Kresse, G.; Joubert, D. *Phys. Rev. B* **1999**, *59*, 1758-1775.

32 Theobald, F.; Laarif, A.; Hewat, A.W. *Mat. Res. Bull.* **1985**, *20*, 653-665.

33 Tyuterev, V.G.; Vast, N. *Comput. Mater. Sci.* **2006**, *38*, 350-353.

34 Wheeler, S.E.; Houk, K.N. *J. Chem. Theory Comput.* **2010**, *6*, 395-404.

[35] Henkelman, G.; Jonsson, H. *J. Chem. Phys.* **2000**, *113*, 9978-9985.

[36] Carducci, M.D.; Brown, C.; Solomon, E.L.; Enemark, J.H. *J. Am. Chem. Soc.* **1994**, *116*, 11856-11868.

[37] Henkelman, G.; Jonsson, H.; *J. Chem. Phys.* **2000**, *113*, 9901-9904.

[38] Shao, Y.; Molnar, L. F.; Jung, Y.; Kussmann, J.; Ochsenfeld, C.; Brown, S. T.; Gilbert, A. T. B.; Slipchenko, L. V.; Levchenko, S. V.; O'Neill, D. P.; DiStasio, R. A., Jr; Lochan, R. C.; Wang, T.; Beran, G. J. O.; Besley, N. A.; Herbert, J. M.; Lin, C. Y.; Van Voorhis, T.; Chien, S. H.; Sodt, A.; Steele, R. P.; Rassolov, V. A.; Maslen, P. E.; Korambath, P. P.; Adamson, R. D.; Austin, B.; Baker, J.; Byrd, E. F. C.; Dachsel, H.; Doerksen, R. J.; Dreuw, A.; Dunietz, B. D.; Dutoi, A. D.; Furlani, T. R.; Gwaltney, S. R.; Heyden, A.; Hirata, S.; Hsu, C.-P.; Kedziora, G.; Khalliulin, R. Z.; Klunzinger, P.; Lee, A. M.; Lee, M. S.; Liang, W.; Lotan, I.; Nair, N.; Peters, B.; Proynov, E. I.; Pieniazek, P. A.; Rhee, Y. M.; Ritchie, J.; Rosta, E.; Sherrill, C. D.; Simmonett, A. C.; Subotnik, J. E.; Woodcock, H. L., III; Zhang, W.; Bell, A. T.; Chakraborty, A. K.; Chipman, D. M.; Keil, F. J.; Warshel, A.; Hehre, W. J.; Schaefer, H. F., III; Kong, J.; Krylov, A. I.; Gill, P. M. W.; Head-Gordon, M. *Phys. Chem. Chem. Phys.* **2006**, *8* (27), 3172–3191.
[39] Krenzke, L.D.; Keulks, G.W. *J. Catal.* **1980**, *61*, 316-325.

[40] Wragg, R.D.; Ashmore, P.G.; Hockey, J.A. *J. Catal.* **1973**, *28,* 337.

[41] Keulks, G.W.; Krenzke, L.D.; Notermann, T.M. *Adv. Catal.* **1978**, *27*, 183-225.

[42] Brazdil, J.F.; Suresh, D.D.; Grasselli, R.K. *J. Catal.* **1980**, *66*, 347-367.

[43] Keulks, G.W. *J. Catal.* **1970**, *19*, 232-235.

[44] Zhai, Z.; Wang, X.; Licht, R.B.; Bell, A.T. *J. Catal.* **2015**, *325*, 87-100.

[45] Stradella, L.; Vogliolo, G. *Z. Phys. Chem.* **1973**, *137*, 99-110.

Table of Contents Figure

ΔE‡ =
+38.8 kcal/mol
$E_{a,app}$ = +27.3 kcal/mol

/mol

+O₂, -H₂O
Bi₂Mo₃O₁₂

NH₃

ΔE‡ =
+23.6 kcal/mol

NH₂

N